Title

Chromatin remodeler CHD4 establishes chromatin states required for ovarian reserve formation, maintenance and male germ cell survival

Journal

Nucleic Acids Research, 53(3)

ISSN

0305-1048

Authors

Munakata, Yasuhisa

Hu, Mengwen

Kitamura, Yuka

et al.

Publication Date

2025-01-24

DOI

10.1093/nar/gkaf008

Peer reviewed

Nucleic Acids Research, 2025, **53**, gkaf008
https://doi.org/10.1093/nar/gkaf008
Advance access publication date: 5 February 2025
Gene regulation, Chromatin and Epigenetics

Chromatin remodeler CHD4 establishes chromatin states required for ovarian reserve formation, maintenance and male germ cell survival

Yasuhisa Munakata [1], Mengwen Hu [1], Yuka Kitamura [1], Raissa G. Dani [1], Adam L. Bynder[1], Amelia S. Fritz[1], Richard M. Schultz[1,2,*] and Satoshi H. Namekawa [1,*]

[1]Department of Microbiology and Molecular Genetics, University of California, Davis, CA 95616, USA
[2]Department of Biology, University of Pennsylvania, Philadelphia, PA 19104, USA

[*]To whom correspondence should be addressed. Tel: +1 530 754 1876; Email: snamekawa@ucdavis.edu
Correspondence may also be addressed to Richard M. Schultz. Email: rschultz@sas.upenn.edu
Present address: Yasuhisa Munakata, Department of Cell Science, Institute of Biomedical Sciences, School of Medicine, Fukushima Medical University, Fukushima, 960-1295, Japan.

Abstract

The ovarian reserve defines female reproductive lifespan, which in humans spans decades due to the maintenance of meiotic arrest in non-growing oocytes (NGOs) residing in primordial follicles. Unknown is how the chromatin state of NGOs is established to enable long-term maintenance of the ovarian reserve. Here, we show that a chromatin remodeler, CHD4, a member of the Nucleosome Remodeling and Deacetylase (NuRD) complex, establishes chromatin states required for formation and maintenance of the ovarian reserve. Conditional loss of CHD4 in perinatal mouse oocytes results in acute death of NGOs and depletion of the ovarian reserve. CHD4 establishes closed chromatin at regulatory elements of pro-apoptotic genes to prevent cell death and at specific genes required for meiotic prophase I to facilitate the transition from meiotic prophase I oocytes to meiotically-arrested NGOs. In male germ cells, CHD4 establishes closed chromatin at the regulatory elements of pro-apoptotic genes, allowing germ cell survival. These results demonstrate a role for CHD4 in defining a chromatin state that ensures germ cell survival, thereby enabling the long-term maintenance of both female and male germ cells.

Graphical abstract

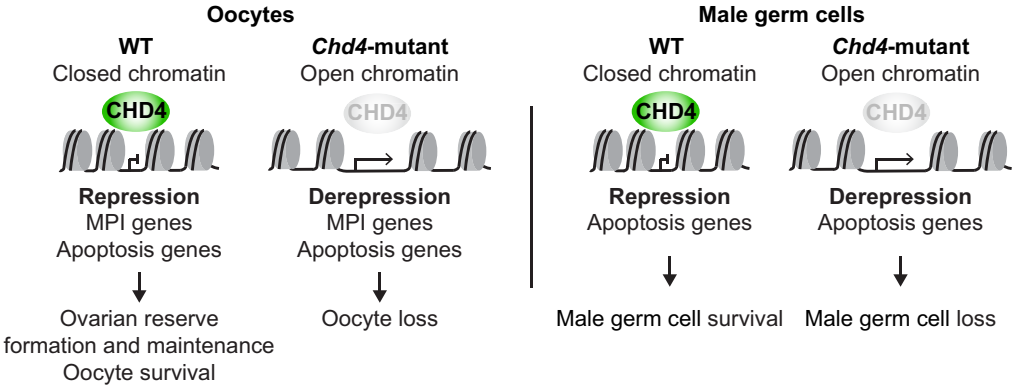

Introduction

Germ cell maintenance and survival are fundamental for the continuous supply of gametes for reproduction. In adult mammals, while the male germline is maintained by self-renewal of spermatogonial stem cells, the female germline is not maintained by a stem cell-based mechanism but is maintained within a pool of meiotically-arrested oocytes, called the ovarian reserve. These small non-growing oocytes (NGOs) residing in primordial follicles are arrested at the dictyate stage, the prolonged diplotene stage, of meiotic prophase I (MPI) (1). NGOs are the only source of fertilizable eggs throughout a female's reproductive life span. Because the number of NGOs is finite, their premature depletion leads to infertility associated with early menopause, such as premature ovarian insufficiency (2). However, the mechanisms underlying formation and maintenance of the ovarian reserve remain largely elusive.

Received: August 23, 2024. **Revised:** December 13, 2024. **Editorial Decision:** December 31, 2024. **Accepted:** January 6, 2025

In the female germline of mouse embryos, primordial germ cells initiate MPI after induction of genes specifically expressed in MPI (MPI genes) (3). After completing chromosome synapsis and recombination, oocytes reach the dictyate stage around birth, gradually decreasing in number before formation of the ovarian reserve (4–6). During ovarian reserve formation, MPI genes are suppressed, and there is a transition in genome-wide transcription to become NGOs, which is termed the perinatal oocyte transition (POT) (7,8). POT is regulated by an epigenetic regulator, Polycomb Repressive Complex 1 (PRC1), to suppress MPI genes when oocytes exit MPI (7). Concomitantly, an oocyte-specific transcription factor FIGLA and several signaling pathways, such as Notch, TGF-β, JNK and hypoxia signaling that regulate gene expression are required for primordial follicle formation (9–13). These studies raise the possibility that the chromatin state in NGOs is uniquely established to instruct the gene expression program for ovarian reserve formation.

To identify a chromatin-based mechanism underlying the process of the ovarian reserve formation and maintenance, we sought to identify a mechanism that generates a unique chromatin state in NGOs. To this end, we examined the role of adenosine triphosphate (ATP)-dependent chromatin remodelers, which use the energy from ATP hydrolysis to reorganize chromatin and regulate gene expression (14,15). There are four major subfamilies of chromatin remodeling complexes, including SWI/SNF (switch/sucrose nonfermentable), ISWI (imitation SWI), NuRD (nucleosome remodeling and deacetylase)/CHD (chromodomain helicase DNA-binding)/mi-2, and INO80/SWR (SWI2/SNF2 related) families (14,15). Among the adenosine triphosphatase (ATPase) subunits in these four major chromatin remodeler subfamilies, we focused our attention on CHD4 (also known as Mi-2β) based on its gene expression at POT and because CHD4 is associated with lineage commitment and differentiation processes (16–19). CHD4 is a core subunit of both the NuRD complex and the ChAHP (CHD4, ADNP, HP1) and ChAHP2 (CHD4, ADNP2, HP1) complexes and functions not only as a transcriptional repressor but also modulates chromatin structure at the sites of active transcription to fine-tune gene expression (20–23). In the male germline, CHD4 regulates maintenance and survival of undifferentiated spermatogonia (24–26). However, the molecular mechanisms underlying this process remain unknown.

Here we show that CHD4 has an essential function in formation and maintenance of the ovarian reserve and determine molecular mechanisms common to both female and male germ cells. In the female germline, CHD4 establishes closed chromatin at regulatory elements of pro-apoptotic genes to prevent cell death and at MPI genes to facilitate the transition from MPI to NGO. Further, in the male germline, CHD4 establishes closed chromatin at the regulatory elements of pro-apoptotic genes, allowing male germ cell survival. Thus, CHD4 defines the chromatin state for maintenance of both female and male germ cells.

Materials and methods

Animals

Generation of conditionally deficient *Chd4* DcKO mice, *Chd4* $^{f/-}$*; Ddx4*-Cre $^{Tg/+}$, were generated from *Chd4*$^{f/f}$ female crossed with *Chd4* $^{f/+}$*; Ddx4*-Cre $^{Tg/+}$ males and *Chd4* Dctrl mice used in experiments were *Chd4*$^{f/+}$*; Ddx4*-Cre $^{Tg/+}$ littermate. Generation of conditionally deficient *Chd4* GcKO mice, *Chd4* $^{f/f}$*; Gdf9*-iCre $^{Tg/+}$, were generated from *Chd4* $^{f/f}$ female crossed with *Chd4* $^{f/f}$*; Gdf9*-iCre $^{Tg/+}$ males and *Chd4* Gctrl mice used in experiments were *Chd4*$^{f/f}$ littermate. Generation of *Chd4* floxed alleles (*Chd4* $^{f/f}$) were reported previously (27). Mice were maintained on a mixed genetic background of C57BL/6 and DBA2. *Ddx4*-Cre transgenic mice were purchased from the Jackson Laboratory (28). For ATAC-seq and Cleavage Under Targets and Tagmentation (CUT&Tag), *Chd4* $^{f/f}$*; Stella*-GFP $^{Tg/+}$ mice were generated from *Chd4* $^{f/f}$ mice crossed with *Stella*-GFP $^{Tg/+}$ mice. *Stella*-GFP transgenic mice were obtained from Dr M. Azim Surani (29). For each experiment, a minimum of three mice was analyzed. Mice were maintained on a 12:12 light: dark cycle in a temperature- and humidity-controlled vivarium (22 ± 2°C; 40–50% humidity) with free access to food and water in the pathogen-free animal care facility. Mice were used according to the guidelines of the Institutional Animal Care and Use Committee (IACUC: protocol no. IACUC 21931 and 23545) at the University of California, Davis.

Oocyte collection

P1, P5 or P10 female pups were collected, and ovaries were harvested by carefully removing oviducts and ovarian bursa in phosphate-buffered saline (PBS). Ovaries were digested in 200 µl TrypLE™ Express Enzyme (1×) (Gibco, 12604013) supplemented with 0.3 mg/ml Collagenase Type 1 (Worthington, CLS-1) and 10 mg/ml DNase I (Sigma, D5025) and incubated at 37°C for 25 min with gentle agitation. After incubation, the ovaries were dissociated by gentle pipetting using the Fisherbrand™ Premium Plus MultiFlex Gel-Loading Tips until no tissue pieces were visible. Two milliliters of Dulbecco's modified Eagle's medium (DMEM)/F-12 medium (Gibco, 11330107) supplemented with 10% fetal bovine serum (FBS) (HyClone, SH30396.03) were then added to the suspension to stop enzyme reaction. Cell suspension was seeded onto a 60 mm tissue culture dish (Falcon, 353002). The cells were allowed to settle down for 15 min at 37°C; 5% CO_2 in the incubator before being transferred under the microscope (Nikon, SMZ1270). For RNA-seq, based on morphology and diameter, NGOs and GOs were manually picked up, washed in M2 medium (Sigma, M7167) and transferred into the downstream buffer with a mouth pipette. For ATAC-seq and CUT&Tag, P1 NGOs expressing a *Stella*-GFP transgene were collected by fluorescence-activated cell sorting (FACS) (SONY SH800S).

Histology and immunostaining

For the preparation of paraffin blocks, ovaries and testis were fixed with 4% paraformaldehyde overnight at 4°C. Ovaries and testis were dehydrated and embedded in paraffin. For histological analysis, 5 µm-thick paraffin sections were deparaffinized and stained with hematoxylin (Sigma, MHS16) and eosin (Sigma, 318906). For immunostaining, 5 µm-thick paraffin sections were deparaffinized and autoclaved in target retrieval solution (DAKO) for 10 min at 121°C. Sections were blocked with Blocking One Histo (Nacalai) for 30 min at room temperature and then incubated with primary antibodies as outlined below: mouse anti-CHD4 (1:500, Abcam, ab70469), rabbit anti-DDX4 (1:500, Abcam, ab13840), goat anti-CD117/c-kit (1:200, R&D, AF1356), rabbit anti-Cleaved Caspase-3 (1:200, Cell Signaling Tech-

nology, #9661), rabbit anti-FOXO3 (1:200, Cell Signaling Technology, #2497), rabbit anti-PUMA/BBC3 (1:500, Abcam, ab9643), rabbit anti-HORMAD1 (1:400, C-terminal antibody: gift from Atilla Toth) overnight at 4°C. Sections were washed with PBST (PBS containing 0.1% Tween 20) three times at room temperature for 5 min and then incubated with the corresponding secondary (Invitrogen) at 1:500 dilution for 1 h at room temperature. Finally, sections were counterstained with 4′,6-diamidino-2-phenylindole (DAPI) and mounted using 20 μl undiluted ProLong Gold Antifade Mountant (ThermoFisher Scientific, P36930). Images were obtained by an all-in-one fluorescence microscope (BZ-X810, KEYENCE) equipped with an optical sectioning module (BZ-H4XF, KEYENCE).

Quantification of ovarian follicles

For counting the number of follicles, paraffin-embedded ovaries were serially sectioned at 5 μm thickness, and all sections were mounted on slides. Five micrometer-thick paraffin serially sections were deparaffinized and stained with hematoxylin and eosin. Ovarian follicles at different developmental stages, including primordial (type 1 and type 2) as NGOs, and primary (type 3) and pre-antral (type 4 and type 5) as GOs, were counted in every fifth section of the collected sections from one ovary, based on the standard established method (30). In each section, only those follicles in which the nucleus of the oocyte was clearly visible were counted, and the cumulative follicle counts were multiplied by a correction factor of 5 to represent the estimated number of follicles in an ovary.

Meiotic chromosome spreads and immunofluorescence

Chromosome spreads of oocytes from neonatal ovaries were prepared as described (7). Briefly, ovaries were digested in 200 μl TrypLE™ Express Enzyme (1×) supplemented with 0.3 mg/ml Collagenase Type 1 and 10 mg/ml DNase I and incubated at 37°C for 25 min with gentle agitation. After incubation, the ovaries were dissociated by gentle pipetting using the Fisherbrand™ Premium Plus MultiFlex Gel-Loading Tips until no visible tissue pieces. Two milliliters of DMEM/F-12 medium supplemented with 10% FBS was added to the suspension to stop enzyme reaction. Cell suspension was incubated in hypotonic extraction buffer [HEB: 30 mM Tris base, 17 mM trisodium citrate, 5 mM ethylenediaminetetraacetic acid, 50 mM sucrose, 5 mM dithiothreitol, 1× cOmplete Protease Inhibitor Cocktail (Sigma, 11836145001), 1× phosphatase inhibitor cocktail 2 (Sigma, P5726-5ML), pH 8.2] on ice for 10 min. Thirty microliters of the suspension was applied to positively charged slides (Probe On Plus: Thermo Fisher Scientific, 22-230-900); before application of the suspension, the slides had been incubated in chilled fixation solution (2% paraformaldehyde, 0.1% Triton X-100, 0.02% sodium monododecyl sulfate, adjusted to pH 9.2 with sodium borate buffer). The slides were placed in humidified chambers overnight at room temperature. Then, the slides were washed twice in 0.4% Photo-Flo 200 (Kodak, 146-4510), 2 min per wash. Slides were dried completely at room temperature before staining or storage in slide boxes at −80°C.

Flow cytometry and cell sorting

Flow cytometric experiments and cell sorting were performed using SH800S (SONY), with antibody-stained testicular single-cell suspensions prepared as described previously. Data were analyzed using SH800S software (SONY) and FCS Express 7 (De Novo Software).

For ATAC-seq and CUT&Tag, P1 oocytes were identified and collected using expression of the *Stella*-GFP transgene. To prepare single cells suspension for cell sorting, ovaries were digested in 200 μl TrypLE™ Express Enzyme (1×) supplemented with 0.3 mg/ml Collagenase Type 1 and 10 mg/ml DNase I and incubated at 37°C for 25 min with gentle agitation. After incubation, the ovaries were dissociated by gentle pipetting using the Fisherbrand™ Premium Plus MultiFlex Gel-Loading Tips until no visible tissue pieces. Two milliliters of DMEM/F-12 medium supplemented with 10% FBS was added to the suspension to stop enzyme reaction. Cells were suspended in FACS buffer (PBS containing 2% FBS) and filtered into a 5 ml FACS tube through a 35 μm nylon mesh cap (Falcon, 352235). GFP$^+$ oocytes were collected after removing small and large debris in FSC-A versus SSC-A gating and doublets in FSC-W versus FSC-H gating.

Collection of male germ cells was carried out as described in reference (31) with minor modifications. Briefly, to prepare single cells suspension for cell sorting, detangled seminiferous tubules from P3 mouse testes were incubated in 1× Krebs–Ringer Bicarbonate Buffer (Sigma, K4002) supplemented with 1.5 mg/ml Collagenase Type 1 and 0.04 mg/ml DNase I at 37°C for 15 min with gentle agitation and dissociated using vigorous pipetting, and then add 0.75 mg/ml hyaluronidase (Sigma, H3506) and incubate at 37°C for 10 min with gentle agitation and dissociated using vigorous pipetting. Ten milliliters of DMEM/F-12 medium supplemented with 10% FBS was added to the suspension to stop enzyme reaction. The cell suspension was washed with 10 ml FACS buffer three times by centrifugation at 300 × *g* for 5 min and filtered through a 70 μm nylon cell strainer (Falcon, 352350). The cell suspension was stained with cocktails of antibodies diluted with FACS buffer listed as follows: phycoerythrin (PE)-conjugated anti-mouse/human CD324 (E-Cadherin) antibody (1:500, Biolegend, 147303) and fluorescein isothiocyanate (FITC)-conjugated anti-mouse CD9 antibody (1:500, Biolegend, 124808). After 50-min incubation on ice, cells were washed with 10 ml FACS buffer three times by centrifugation at 300 × *g* for 5 min and filtered into a 5 ml FACS tube through a 35 μm nylon mesh cap. 7-AAD Viability Stain (Invitrogen, 00-6993-50) and 0.01 mg/ml DNase I was added to cell suspension for the exclusion of dead cells. Samples were kept on ice until sorting. Cells were analyzed after removing small and large debris in FSC-A versus SSC-A gating, doublets in FSC-W versus FSC-H gating, and 7AAD$^+$ dead cells. Then, the desired cell population was collected in gates and determined based on antibody staining.

RNA-seq library generation and sequencing

RNA-seq libraries of oocytes from P1, P5 and P10 ovaries were prepared as described (7); briefly, 500 NGOs and 100 GOs isolated from ovaries were pooled as one replicate, and two independent biological replicates were used for RNA-seq library generation. Total RNA was extracted using the RNeasy Plus Micro Kit (QIAGEN, Cat # 74034) according to the manufacturer's instructions. Library preparation was performed with NEBNext® Single Cell/Low Input RNA Library Prep Kit for Illumina® (NEB, E6420S) according to the manufacturer's instruction. Prepared RNA-seq libraries were se-

quenced on the HiSeq X system (Illumina) with paired-ended 150-bp reads.

ATAC-seq library generation and sequencing

ATAC-seq libraries of germ cells were prepared as described (32); briefly, 10,000 FACS-sorted cells were isolated from P1 ovaries or P3 testis and pooled as one replicate, and two independent biological replicates were used for ATAC-seq library generation. Samples were lysed in 50 μl of lysis buffer [10 mM Tris–HCl (pH 7.4), 10 mM NaCl, 3 mM $MgCl_2$ and 0.1% NP-40, 0.1% Tween-20, and 0.01% Digitonin] on ice for 10 min. Immediately after lysis, the samples were spun at 500 × *g* for 10 min at 4°C and the supernatant removed. The sedimented nuclei were then incubated in 10 μl of transposition mix {0.5 μl homemade Tn5 transposase (~1 μg/μl), 5 μl 2× tagment DNA buffer [10 mM Tris–HCl (pH 7.6), 10 mM $MgCl_2$ and 20% dimethyl formamide], 3.3 μl PBS, 0.1 μl 1% digitonin, 0.1 μl 10% Tween-20 and 1 μl water} at 37°C for 30 min in a thermomixer with shaking at 500 rpm. After tagmentation, the transposed DNA was purified with a MinElute kit (Qiagen). Polymerase chain reaction (PCR) was performed to amplify the library using the following conditions: 72°C for 3 min; 98°C for 30 s; thermocycling at 98°C for 10 s, 60°C for 30 s and 72°C for 1 min. Quantitative PCR was used to estimate the number of additional cycles needed to generate products at 25% saturation. Seven to eight additional PCR cycles were added to the initial set of five cycles. Amplified DNA was purified by SPRIselect bead (Beckman Coulter). ATAC-seq libraries were sequenced on the HiSeq X Ten system (Illumina) with 150-bp paired-end reads.

CUT&Tag library generation and sequencing

CUT&Tag libraries from P1 oocytes for CHD4 were generated as previously described (33,34) (a step-by-step protocol https://dx.doi.org/10.17504/protocols.io.bcuhiwt6) using CUTANA™ pAG-Tn5 (Epicypher, 15-1017). Briefly, 10,000 FACS-sorted cells were isolated from P1 *Chd4 f/f* ovaries and pooled as one replicate and two independent biological replicates were used for CUT&Tag library generation. The antibodies used were mouse anti-CHD4 (1:50, Abcam, ab70469) and rabbit α-mouse antibody (1:100, Abcam, ab46540). CUT&Tag libraries were sequenced on the NovaSeq X Plus system (Illumina) with 150-bp paired-end reads.

RNA-seq data processing

Raw paired-end RNA-seq reads after trimming by trimmomatic (version 0.39) (35) were aligned to the mouse (GRCm38/mm10) genome using STAR (version STAR_2.5.4b) (36) with default arguments. All unmapped and non-uniquely mapped reads were filtered out by samtools (version 1.9) (37) before being subjected to downstream analyses. To quantify aligned reads in RNA-seq, aligned read counts for each gene were generated using featureCounts (v2.0.1), which is part of the Subread package (38) based on annotated genes (GENCODE vM25). The transcripts per million (TPM) values of each gene were for comparative expression analyses and computing the Pearson correlation coefficient between biological replicates using corrplot (39).

To detect differentially expressed genes (DEGs) between *Chd4* Dctrl and *Chd4* DcKO, or *Chd4* Gctrl and *Chd4* GcKO, DESeq2 (version 1.42.1) (40) was used for differential gene expression analyses with cutoffs ≥2-fold change and binominal tests (*Padj* < 0.05; *P*-values were adjusted for multiple testing using the Benjamini–Hochberg method). *Padj* values were used to determine significantly dysregulated genes.

To perform Gene Ontology analyses, we used the online functional annotation clustering tool Metascape (41) (http://metascape.org). Further analyses were performed with R and visualized as heatmaps using Morpheus (https://software.broadinstitute.org/morpheus, Broad Institute).

ATAC-seq and CUT&Tag data processing

Raw paired-end ATAC-seq and CUT&Tag reads after trimming by Trim-galore (https://github.com/FelixKrueger/TrimGalore) (version 0.6.7) were aligned to either the mouse (GRCm38/mm10) genomes using bowtie2 (version 2.3.3.1) (42) with default arguments. The aligned reads were filtered to remove alignments mapped to multiple locations by calling grep with the -v option before being subjected to downstream analyses. PCR duplicates were removed using the 'MarkDuplicates' command in Picard tools (version 2.23.8) (https://broadinstitute.github.io/picard/, Broad Institute). To compare replicates, Pearson correlation coefficients were calculated and plotted by 'multiBamSummary bins' and 'plot correlation' functions of deepTools (version 3.3.0) (43). Biological replicates were pooled for visualization and other analyses after validation of reproducibility. Peak calling for ATAC-seq and CUT&Tag data was performed using MACS3 (version 3.0.0a7) (44) with default arguments. We computed the number of overlapping peaks between peak files using BEDtools (45) (version 2.28.0) function intersect. To detect genes adjacent to ATAC-seq and CUT&Tag peaks, we used the HOMER (version 4.9.1) (46) function annotatePeaks.pl. The deeptools (43) was used to draw tag density plots and heatmaps for reads enrichments. To visualize ATAC-seq and CUT&Tag data using the Integrative Genomics Viewer (Broad Institute) (47), bins per million (BPM) normalized counts data were created from sorted BAM files using the deeptools (43). To perform functional annotation enrichment of CHD4, we used GREAT tools (48).

Statistics

Statistical methods and *P*-values for each plot are listed in the figure legends and/or in the 'Materials and methods' section. In brief, all grouped data are represented as mean ± standard deviation (SD). All box-and-whisker plots are represented as center lines (median), box limits [interquartile range (IQR); 25th and 75th percentiles] and whiskers (maximum value not exceeding 1.5× the IQR from the hinge) unless stated otherwise. Statistical significance for pairwise comparisons was determined using two-sided Mann–Whitney U-tests and two-tailed unpaired *t*-tests. Next-generation sequencing data (RNA-seq, ATAC-seq and CUT&Tag) were based on two independent replicates. No statistical methods were used to predetermine sample size in these experiments. Experiments were not randomized, and investigators were not blinded to allocation during experiments and outcome assessments.

Code availability

Source code for all software and tools used in this study with documentation, examples and additional information is available at the URLs listed below.

trimmomatic [http://www.usadellab.org/cms/?page=trimmomatic]

STAR [https://github.com/alexdobin/STAR]
featureCounts [http://subread.sourceforge.net]
DESeq2 [https://bioconductor.org/packages/release/bioc/html/DESeq2.html]
corrplot [https://github.com/taiyun/corrplot]
ggplot2 [https://github.com/tidyverse/ggplot2]
Metascape [http://metascape.org]
Morpheus [https://software.broadinstitute.org/morpheus/]
Trim-galore [https://github.com/FelixKrueger/TrimGalore]
Bowtie2 [https://github.com/BenLangmead/bowtie2]
Picard [https://broadinstitute.github.io/picard/]
deepTools [https://github.com/deeptools/deepTools]
MACS3 [https://github.com/macs3-project/MACS]
Bedtools [https://github.com/arq5x/bedtools2]
HOMER [http://homer.ucsd.edu/homer/index.html]
GREAT [http://great.stanford.edu/public/html/]

Results

CHD4 is required for ovarian reserve formation

To identify a key ATP-dependent chromatin remodeler that functions in ovarian reserve formation in mice, we compared gene expression profiles of ATPase subunits in representative chromatin remodeler subfamilies using previously published RNA-seq data (13). Among these candidates, *Chd4* is highly expressed from embryonic day 14 (E14.5) oocytes in MPI to postnatal day 4 (P4) and P6 NGOs, which corresponds to the time of ovarian reserve formation when genome-wide gene expression changes occur during POT (7) (Figure 1A). *Chd4* expression was slightly downregulated when NGOs in primordial follicle (labeled as 'small' in Figure 1A) are activated to become GOs in primary follicles (labeled as 'large' in Figure 1A); this transition is termed the primordial to primary follicle transition (13), and the first wave occurs as early as P4 (Figure 1A). Concomitant with the expression of *Chd4* during perinatal oogenesis, genes encoding other components of the NuRD and ChAHP/ChAHP2 complex, such as *Hdac1*, *Hdac2*, *Mta1*, *Mta2* and *Cbx1* were highly expressed during perinatal oogenesis (Supplementary Figure S1A). Based on this gene expression profile, we focused on CHD4 and sought to determine the function of CHD4 in ovarian reserve formation.

To determine the function of CHD4 in ovarian reserve formation, we generated *Chd4* conditional knockout mice using the *Chd4* floxed allele (27) and the *Ddx4*-Cre transgene, which is a germline-specific Cre line expressed from E15.5 (28) (*Chd4*$^{f/-}$; *Ddx4*-Cre $^{Tg/+}$; termed *Chd4* DcKO, Figure 1B). CHD4 protein localized in the nucleus of the P1 oocytes in littermate controls (*Chd4*$^{f/+}$; *Ddx4*-Cre $^{Tg/+}$; termed *Chd4* Dctrl), but was absent in 98.8% of the P1 oocyte nuclei of *Chd4* DcKO mice (Figure 1C and D), confirming the efficient depletion of CHD4 protein in *Chd4* DcKO oocytes. The estimated oocyte number of *Chd4* DcKO neonatal mice at P1 did not differ from that of *Chd4* Dctrl (Figure 1E and F). However, by P5, when the ovarian reserve is established, the estimated oocyte number of *Chd4* DcKO newborn mice was markedly reduced compared to *Chd4* Dctrl (Figure 1E and F). Apoptosis was likely responsible for the loss of oocytes in *Chd4* DcKO newborn mice because immunofluorescence staining for cleaved Caspase 3, a marker of apoptosis, revealed no difference in the proportion of cleaved Caspase 3-positive oocytes in P1, whereas the proportion of cleaved Caspase 3-positive oocytes in P3 *Chd4* DcKO ovaries was significantly increased compared to *Chd4* Dctrl (Figure 2A and B). These results suggest that CHD4 is critical for ovarian reserve formation.

We next examined whether the ovarian reserve is properly established in *Chd4* DcKO ovaries. During the formation of NGOs in the ovarian reserve, localization of the transcription factor FOXO3 changes from the cytoplasm to the nucleus (49); nuclear localization of FOXO3 is a hallmark of NGOs (49). Immunofluorescence staining for FOXO3 showed that in P1 FOXO3 was localized in the cytoplasm of most oocytes in both *Chd4* Dctrl and *Chd4* DcKO (Figure 2C and D). However, at P3, FOXO3 was localized in the nucleus of 92.9% of oocytes in *Chd4* Dctrl whereas nuclear localization was only 7.9% of oocytes in *Chd4* DcKO had FOXO3 (Figure 2C and D). Therefore, NGOs are not properly generated in *Chd4* DcKO ovaries. Nevertheless, the behavior of meiotic chromosomes in MPI, including progression to the dictyate stage of MPI, appeared normal in *Chd4* DcKO (Supplementary Figure S1B). Thus, cell death is not initiated by defects in meiotic chromosome behavior.

CHD4 represses MPI genes and apoptosis genes in ovarian reserve formation

To further examine the function of CHD4 in ovarian reserve formation, NGOs were isolated from P1 and P5 ovaries, and RNA-seq analysis was performed (Supplementary Figure S1C). In P1 *Chd4* DcKO NGOs, 533 genes were upregulated, and 348 genes were downregulated [Figure 3A (left) and Supplementary Dataset S1]. In P5 *Chd4* DcKO NGOs, 569 genes were upregulated, and 396 genes were downregulated [Figure 3A (right) and Supplementary Dataset S2]. To infer possible functions of these DEGs, we performed Gene Ontology enrichment analyses. The genes downregulated in P1 and P5 *Chd4* DcKO oocytes were enriched with genes involved in 'oogenesis' and 'female gamete generation'. On the other hand, the genes upregulated in P5 *Chd4* DcKO oocytes were enriched with genes involved in MPI, such as 'homologous chromosome pairing at meiosis' (Figure 3B), suggesting that CHD4 represses MPI genes. During ovarian reserve formation, MPI genes are repressed as oocytes exit from MPI and the fetal program (7). Therefore, we examined how MPI genes are regulated in *Chd4* DcKO NGOs.

In a previous study (50), 104 genes were identified to be MPI-specific genes in fetal oocytes (50). The expression of these MPI genes is comparable between *Chd4* DcKO and *Chd4* Dctrl NGOs at P1 (Figure 3C). In contrast, in P5 NGOs, expression of MPI genes was significantly upregulated in *Chd4* DcKO relative to *Chd4* Dctrl (Figure 3C). Among them, 23 MPI genes, such as *Spo11* (51,52), *Sycp1* (53), *Hormad1* (54–56), *Meiob* (57) and *Majin* (58), which are important for MPI progression, were included in the DEGs in P5 NGOs (Figure 3D). Because there is a genome-wide gene expression change in POT in normal oogenesis (7), we next examined how DEGs at POT are regulated in the *Chd4* DcKO NGOs. In P5 *Chd4* DcKO NGOs, upregulated genes at POT were downregulated, while downregulated genes at POT were upregulated (Supplementary Figure S1D and E, and Supplementary Dataset S3), further confirming that POT is defective in accordance with defective ovarian reserve formation.

We also examined the expression of the genes in the mouse apoptosis pathway defined in the Kyoto Encyclopedia of

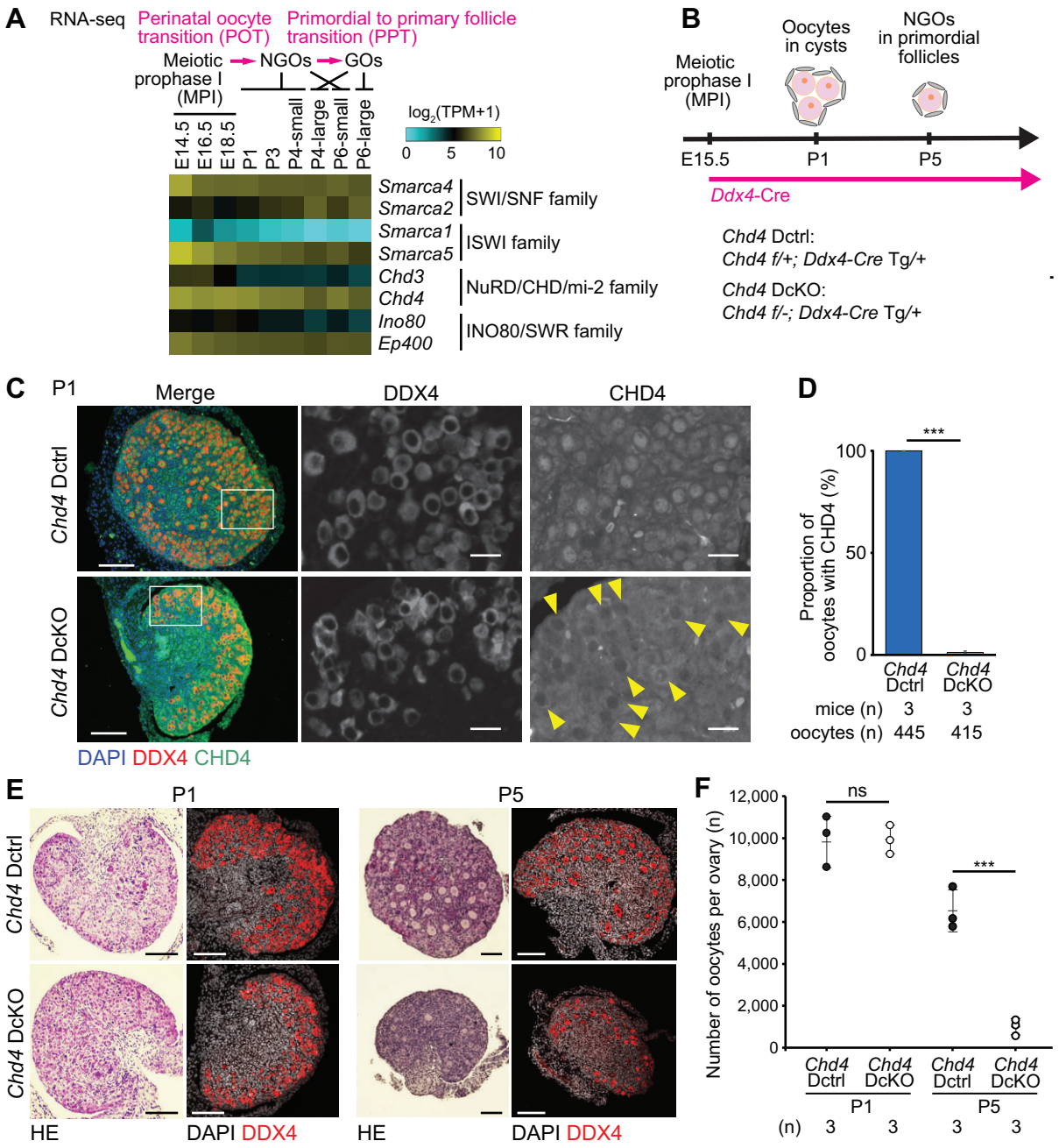

Figure 1. CHD4 deficiency causes oocyte loss. (**A**) Heatmap showing RNA-seq gene expression for core subunits of ATP-dependent remodeling complexes in oocytes during oogenesis. Previously published data (13) were reanalyzed. Embryonic day (**E**) 18.5 to postnatal day (P) 3 indicate oocytes transitioning from MPI to NGOs. P4 and P6 small indicate NGOs residing in primordial follicles. P4 and P6-large indicate GOs in primary follicles. (**B**) Schematic for mouse models and experiments. (**C**) Immunostaining of DDX4 and CHD4 in ovaries of *Chd4* Dctrl and *Chd4* DcKO at P1. CHD4 is present only in somatic cells in *Chd4* DcKO. Bars: 100 μm (20 μm in the boxed area). Arrowheads indicate oocytes with no CHD4 expression. (**D**) Quantitative analysis of immunostaining. Percentages representing numbers of oocytes with CHD4 at P1. Data are presented as mean values ± SD. ***$P < 0.001$: Two-tailed unpaired *t*-tests. Three independent biological replicates were analyzed for each genotype. (**E**) Ovarian sections of *Chd4* Dctrl and *Chd4* DcKO mice at P1 and P5. The sections were stained with hematoxylin and eosin or immunostained for DDX4. Bars: 100 μm. Three mice were analyzed for each genotype at each time point, and representative images are shown. (**F**) Dot plots showing the estimated numbers of oocytes per ovary from *Chd4* Dctrl and *Chd4* DcKO mice at P1 and P5. At least three mice were analyzed for each genotype at each time point. Central bars represent mean values. ***$P < 0.001$: ns, not significant; two-tailed unpaired *t*-tests.

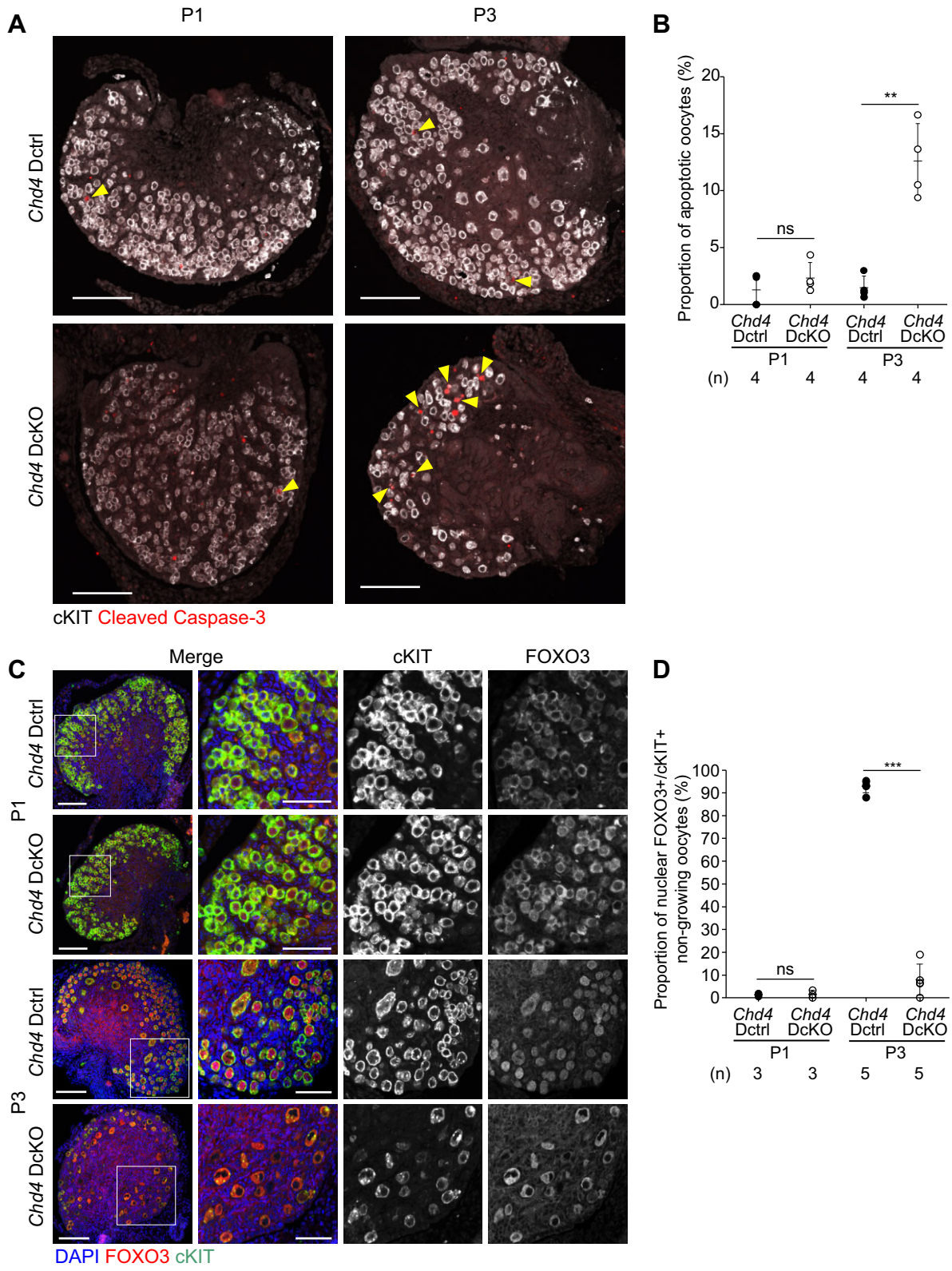

Figure 2. CHD4 is required for ovarian reserve formation. (**A**) Immunostaining of cKIT and Cleaved Caspase-3 in ovaries of *Chd4* Dctrl and *Chd4* DcKO at P1 and P3. Arrowheads indicate Cleaved Caspase-3$^+$ apoptotic oocytes. Bars: 100 μm. Three mice were analyzed for each genotype at each time point, and representative images are shown. (**B**) Quantitative analysis of immunostaining. Dot plots showing the percentages of cleaved Caspase-3$^+$ apoptotic oocytes per cKIT$^+$ oocytes at P1 and P3. Four independent biological replicates were analyzed for each genotype at each time point. $^{**}P < 0.01$: ns, not significant; two-tailed unpaired *t*-tests. (**C**) Immunostaining of FOXO3 and cKIT in ovaries of *Chd4* Dctrl and *Chd4* DcKO at P1 and P5. Bars: 100 μm (50 μm in the boxed area). Three and five mice were analyzed for each genotype at each time point, and representative images are shown. (**D**) Quantitative analysis of immunostaining. Dot plots showing the percentages of nuclear FOXO3$^+$ oocytes per cKIT$^+$ oocytes at P1 and P5, respectively. Three and five independent biological replicates were analyzed for each genotype at each time point. $^{***}P < 0.001$; ns, not significant; two-tailed unpaired *t*-tests.

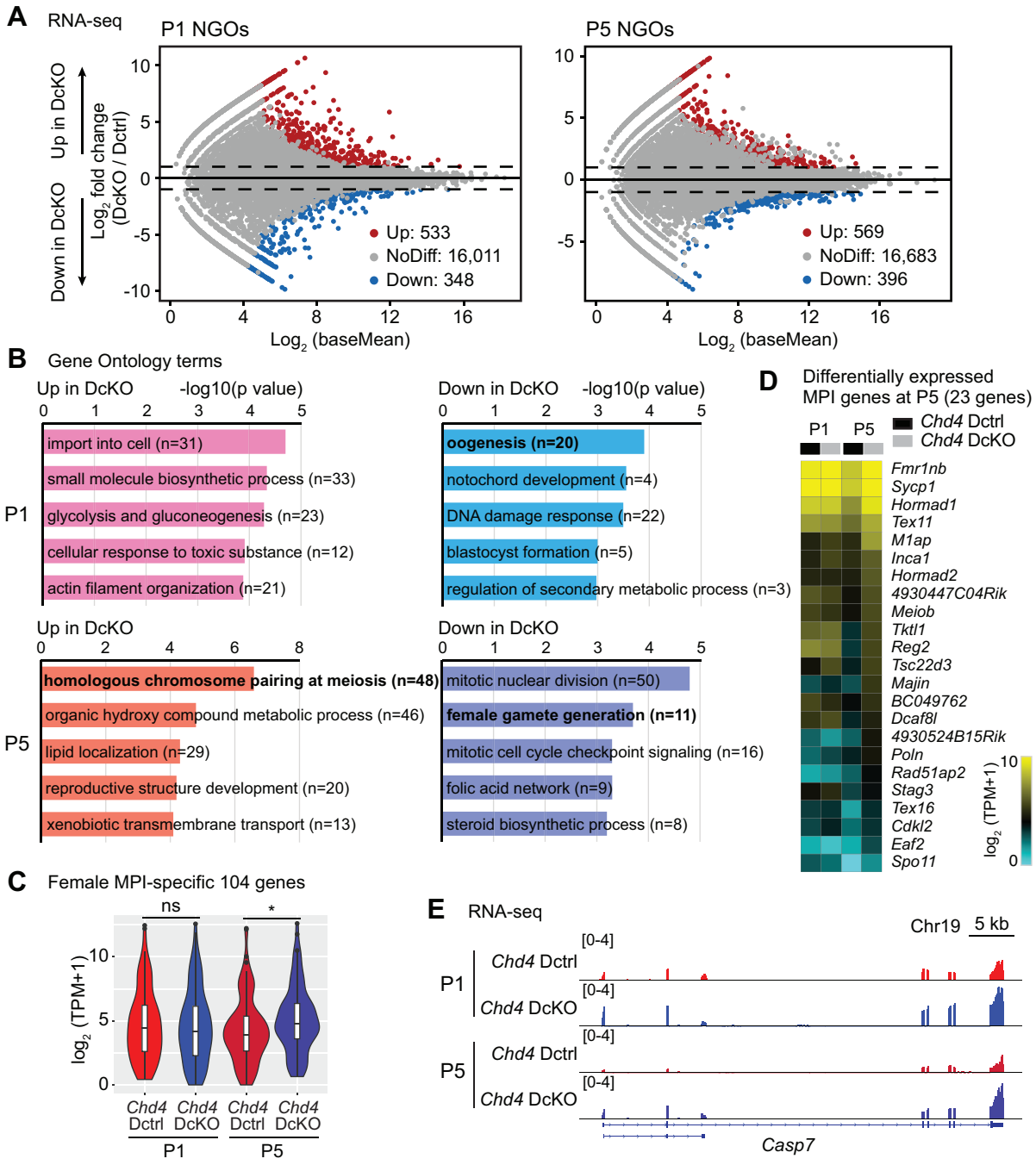

Figure 3. CHD4 represses meiotic prophase I genes and apoptosis-related genes. (**A**) Comparison of RNA-seq data between *Chd4* Dctrl and *Chd4* DcKO oocytes at P1 and P5. A total of 500 NGOs isolated from P1 or P5 ovaries were pooled as one replicate, and two independent biological replicates were examined for RNA-seq. DEGs (Log_2FoldChange > 1, *Padj* < 0.05, binominal test with Benjamini–Hochberg correction) are defined upregulated or downregulated in *Chd4* DcKO oocytes. (**B**) Gene ontology term enrichment analysis of DEGs detected in panel (A). The number of genes in each term is shown. (**C**) Violin plots with a Box plot indicate TPM values for female MPI-specific genes (104 genes) in *Chd4* Dctrl and *Chd4* DcKO oocytes at P1 and P5. The central lines represent medians. The upper and lower hinges correspond to the 25th and 75th percentiles. The upper and lower whiskers are extended from the hinge to the largest value no further than the 1.5× IQR from the hinge. *$P < 0.05$: ns, not significant; Wilcoxon rank sum test. (**D**) Heatmap showing the expression of differentially expressed MPI-specific genes in P5 *Chd4* DcKO oocytes at P1 and P5. (**E**) RNA-seq track views at the *Casp7* gene locus. The y-axis represents normalized tag counts for bulk RNA-seq in each sample. Data ranges are shown in brackets.

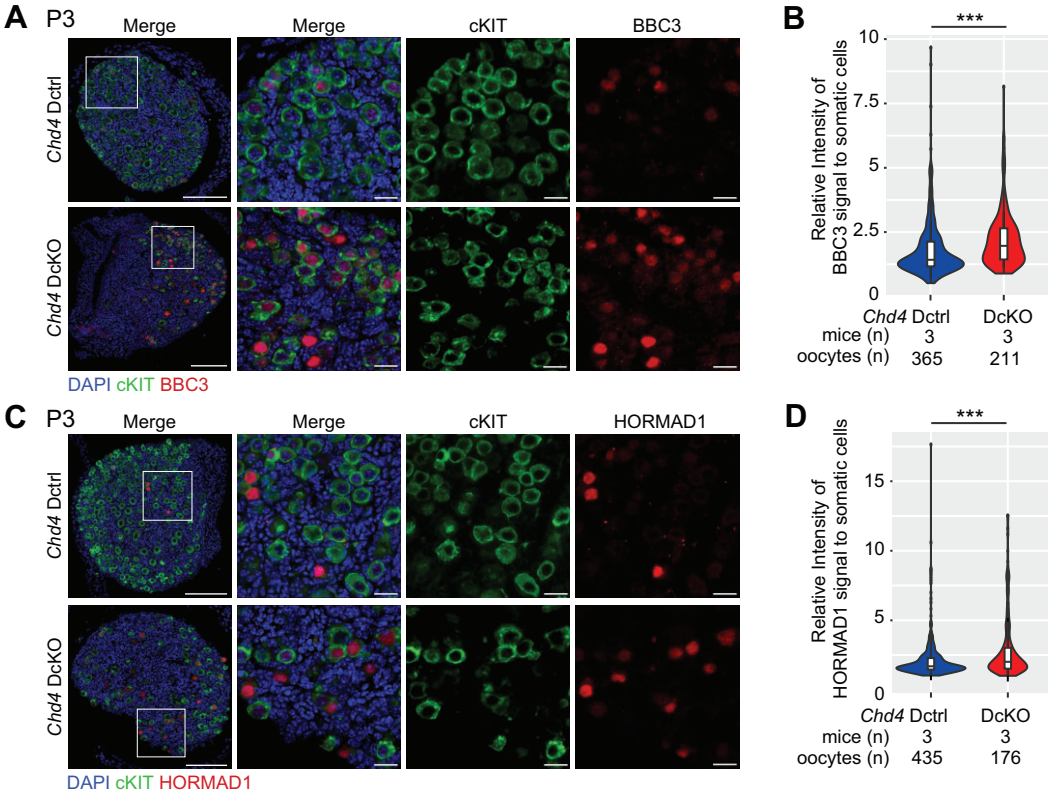

Figure 4. CHD4 represses BBC3 and HORMAD1 in NGOs. (**A, C**) Immunostaining of BBC3 (A) or HORMAD1 (C) and cKIT in ovaries of *Chd4* Dctrl and *Chd4* DcKO at P3. Boxed areas are magnified to the right panels. Bars: 100 μm (20 μm in the boxed areas). (**B, D**) Quantitative analysis of immunostaining. Violin plots with a box plot indicate the BBC3 (**B**) or HORMAD1 (**D**) signal intensity in NGOs relative to somatic cells for *Chd4* Dctrl and *Chd4* DcKO at P3. The central line represents the median. The upper and lower hinges correspond to the 25th and 75th percentiles. The upper and lower whiskers are extended from the hinge to the largest value no further than the 1.5× IQR from the hinge. ***$P < 0.001$: Mann–Whitney U test. Three independent biological replicates were analyzed for each genotype.

Genes and Genomes (KEGG) database (59). Both in P1 and P5 *Chd4* DcKO NGOs, *Casp7*, a gene important for apoptosis (60), was significantly upregulated (Figure 3E). In addition, the pro-apoptotic *Bbc3* (also known as *Puma*) and *Pmaip1* (also known as *Noxa*) genes, which are direct targets of P63 and directly induce apoptosis in oocytes (61–64), were derepressed in the *Chd4* DcKO NGOs (Supplementary Figure S1F). We further performed immunostaining and confirmed that BBC3/PUMA and HORMAD1 protein expression were upregulated in *Chd4* DcKO NGOs at P3 (Figure. 4A–D). Taken together, CHD4 is required for the repression of MPI genes and apoptosis genes during ovarian reserve formation.

CHD4 represses chromatin accessibility to downregulate genes

Because CHD4 represses transcription and chromatin accessibility in various cell types (16,65,66), we next sought to determine how CHD4 regulates chromatin accessibility during ovarian reserve formation. We used the assay for transposase-accessible chromatin by sequencing (ATAC-seq) (32,67) to assess the effect of CHD4 loss on chromatin accessibility in ovarian reserve formation (Supplementary Figure S2A). A representative track view confirms that peak patterns are consistent between two biological replicates (Supplementary Figure S2B). An ATAC-seq analysis of P1 NGOs showed that accessibility was markedly increased in *Chd4* DcKO (Figure 5A). These increased accessibility regions are mainly introns and intergenic regions, and a relatively minor change was observed at promoters and transcription termination sites (Figure 5B). This result suggests that CHD4 regulates distal *cis*-regulatory elements such as enhancers.

Next, we examined the relationship between changes in the distal accessible regions and changes in gene expression following CHD4 loss. Expression of 2906 genes adjacent to *Chd4* Dctrl-specific distal accessible regions (outside the TSSs ±1 kb window) was similar between *Chd4* DcKO and *Chd4* Dctrl NGOs both in P1 and P5 (Figure 5C). However, expression of 5423 genes adjacent to *Chd4* DcKO-specific distal accessible regions was globally upregulated in *Chd4* DcKO NGOs both in P1 and P5 (Figure 5D). Therefore, CHD4 represses distal accessible regions to downregulate genes. Further, we examined chromatin accessibility at the promoters of DEGs in *Chd4* DcKO NGOs. We found that upregulated genes in *Chd4* DcKO NGOs are associated with increased accessibility at promoters both in P1 and P5, whereas downregulated genes were not associated with changes in chromatin accessibility (Figure 5E–H). Chromatin accessibility was increased at the TSS of genes whose expression was upregulated in *Chd4* DcKO; for example, an apoptotic gene *Casp7*, and an MPI gene *Stra8*, which is the transcription factor critical for MPI gene expression (68) (Figure 5I). Together, we conclude that CHD4 represses chromatin accessibility both at promoters and distal regulatory elements to repress genes in ovarian reserve formation.

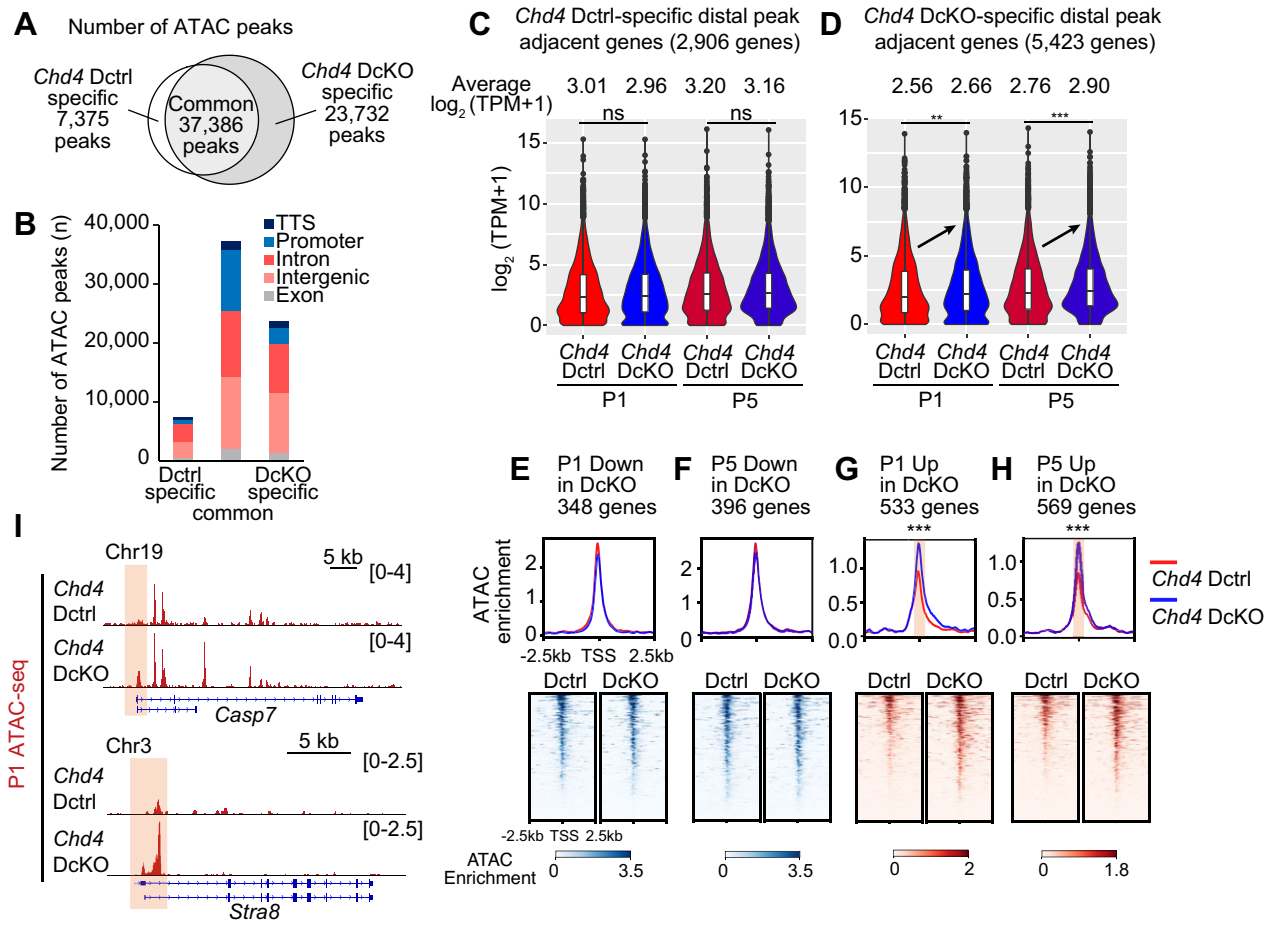

Figure 5. CHD4-dependent regulation of accessible chromatin in perinatal oocytes. (**A**) Venn diagram indicates overlap of ATAC-seq peaks between *Chd4* Dctrl and *Chd4* DcKO oocytes at P1. (**B**) Numbers and genomic distribution of ATAC-seq peaks shown in panel (A). (**C, D**) Violin plots with a box plot indicate changes in TPM values of genes adjacent to specific ATAC-seq peaks in *Chd4* Dctrl (**C**) and *Chd4* DcKO (**D**) oocytes at P1. The central lines represent medians. The upper and lower hinges correspond to the 25th and 75th percentiles. The upper and lower whiskers are extended from the hinge to the largest value no further than the 1.5× IQR from the hinge. ***$P < 0.001$; **$P < 0.01$; ns, not significant; Wilcoxon rank sum test. (**E–H**) Heatmaps and average tag density plots of ATAC-seq enrichment around transcription start sites (TSSs) (±2.5 kb) of downregulated in *Chd4* DcKO oocytes at P1 (**E**) and P5 (**F**) and upregulated in *Chd4* DcKO oocytes at P1 (**G**) and P5 (**H**). ***$P < 0.001$; Wilcoxon rank sum test. (**I**) Representative track views of *Casp7* and *Stra8* gene loci show ATAC-seq signals in *Chd4* Dctrl and *Chd4* DcKO oocytes at P1. The y-axis represents normalized tag counts for ATAC-seq in each sample. The regions around TSSs are highlighted.

CHD4 binds chromatin to regulate MPI and apoptosis genes

Because CHD4 deficiency causes a massive increase in chromatin accessibility, we hypothesized that CHD4 directly binds target sites to regulate chromatin accessibility. To test this hypothesis, we performed CUT&Tag analysis (33) on CHD4 using P1 oocytes to determine where CHD4 is bound in the genome (Supplementary Figure S2C). CUT&Tag analysis revealed that the majority of CHD4 peaks were enriched in introns and intergenic regions (Figure 6A). In addition, most of the CHD4 peaks were located 5–500 kb away from the TSSs (Figure 6B), consistent with the genomic sites of accessibility changes in *Chd4* DcKO NGOs. We compared the ATAC peaks with the CHD4 peaks and found that, surprisingly, only a minor portion of them overlapped (Supplementary Figure S2D), and this is the case for the ATAC distal peaks (Figure 6C). We compared the adjacent gene expression near the CHD4 peaks and found that it was significantly increased in P5 *Chd4* DcKO (Figure 6D), suggesting that CHD4 binds to repress target genes. However, counterintuitively, the CHD4 signals were enriched at the TSSs of the gene that was significantly downregulated in P1 and P5 *Chd4* DcKO (Figure 6E). These results suggest that CHD4 not only directly regulates chromatin accessibility but may also regulate gene expression without changing chromatin accessibility.

To further elucidate the function of CHD4 in formation of ovarian reserve, we focused on apoptosis-associated genes and MPI genes whose expression was upregulated in *Chd4* DcKO NGOs. CHD4 was enriched in the TSSs of the respective gene groups compared to randomly selected regions (Figure 6F and G). At the *Stra8* gene locus, CHD4 binds the TSS, where chromatin accessibly increased in the *Chd4* DcKO NGOs (Figure 6H, left). Furthermore, at the *Bbc3* gene locus, CHD4 bound not only at the TSS but also at the upstream region where chromatin accessibility was increased in *Chd4* DcKO NGOs (Figure 6H, right). Thus, for some important target genes, CHD4 directly regulates chromatin accessibility, supporting a model in which CHD4 represses expression by regulating chromatin accessibility.

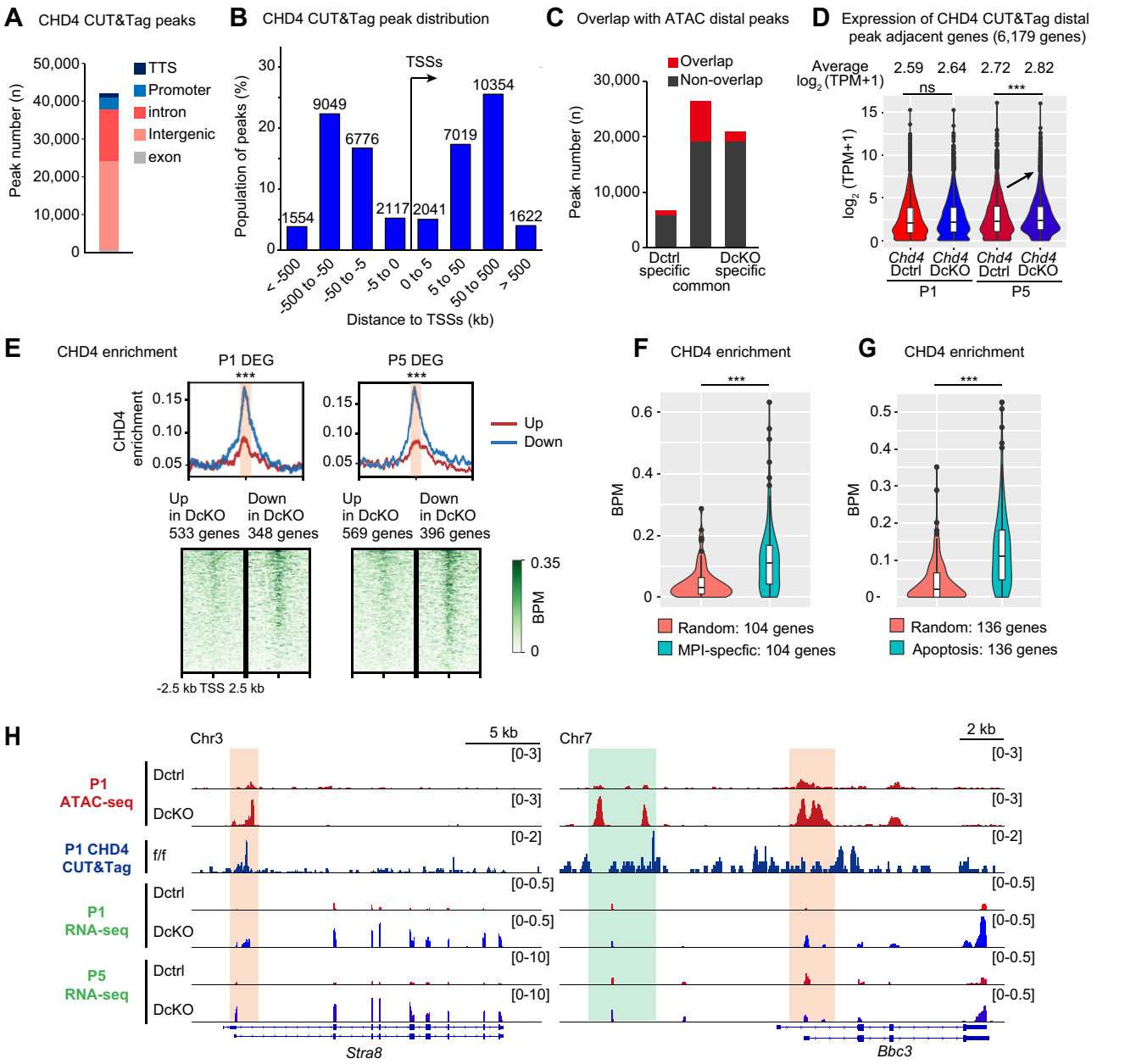

Figure 6. CHD4 binding sites in NGOs at P1. (**A**) Numbers and genomic distribution of CHD4 CUT&Tag peaks in *Chd4*$^{f/f}$ oocytes at P1. (**B**) Bar chart depicts the regional distribution of CHD4 CUT&Tag peaks in each distance range to TSSs. (**C**) Overlap between ATAC distal peaks (>1 kb from TSSs) and CHD4 CUT&Tag peaks in each category. (**D**) Violin plots with a box plot indicate changes in TPM values of genes adjacent to CHD4 CUT&Tag peaks in *Chd4* Dctrl and *Chd4* DcKO oocytes at P1 and P5. The central lines represent medians. The upper and lower hinges correspond to the 25th and 75th percentiles. The upper and lower whiskers are extended from the hinge to the largest value no further than the 1.5× IQR from the hinge. ***$P < 0.001$; ns, not significant; Wilcoxon rank sum test. (**E**) Heatmaps and average tag density plots of CHD4 enrichment around TSS (±2.5 kb) of DEG in *Chd4* Dctrl and *Chd4* DcKO oocytes at P1 and P5. ***$P < 0.001$; Wilcoxon rank sum test. (**F, G**) Violin plots with a box plot indicate CHD4 enrichment around TSS (±1 kb) for female MPI-specific genes [(**F**) 104 genes] and apoptosis pathway genes in the KEGG database [(**G**) 136 genes] in *Chd4* Dctrl and *Chd4* DcKO oocytes at P1 and P5. The central lines represent medians. The upper and lower hinges correspond to the 25th and 75th percentiles. The upper and lower whiskers are extended from the hinge to the largest value no further than the 1.5× IQR from the hinge. ***$P < 0.001$; Wilcoxon rank sum test. (**H**) Representative track views of the *Stra8* and *Bbc3* loci in P1 and P5 oocytes of indicated genotypes. Data ranges are shown in brackets. Putative promoter and enhancer regions are highlighted.

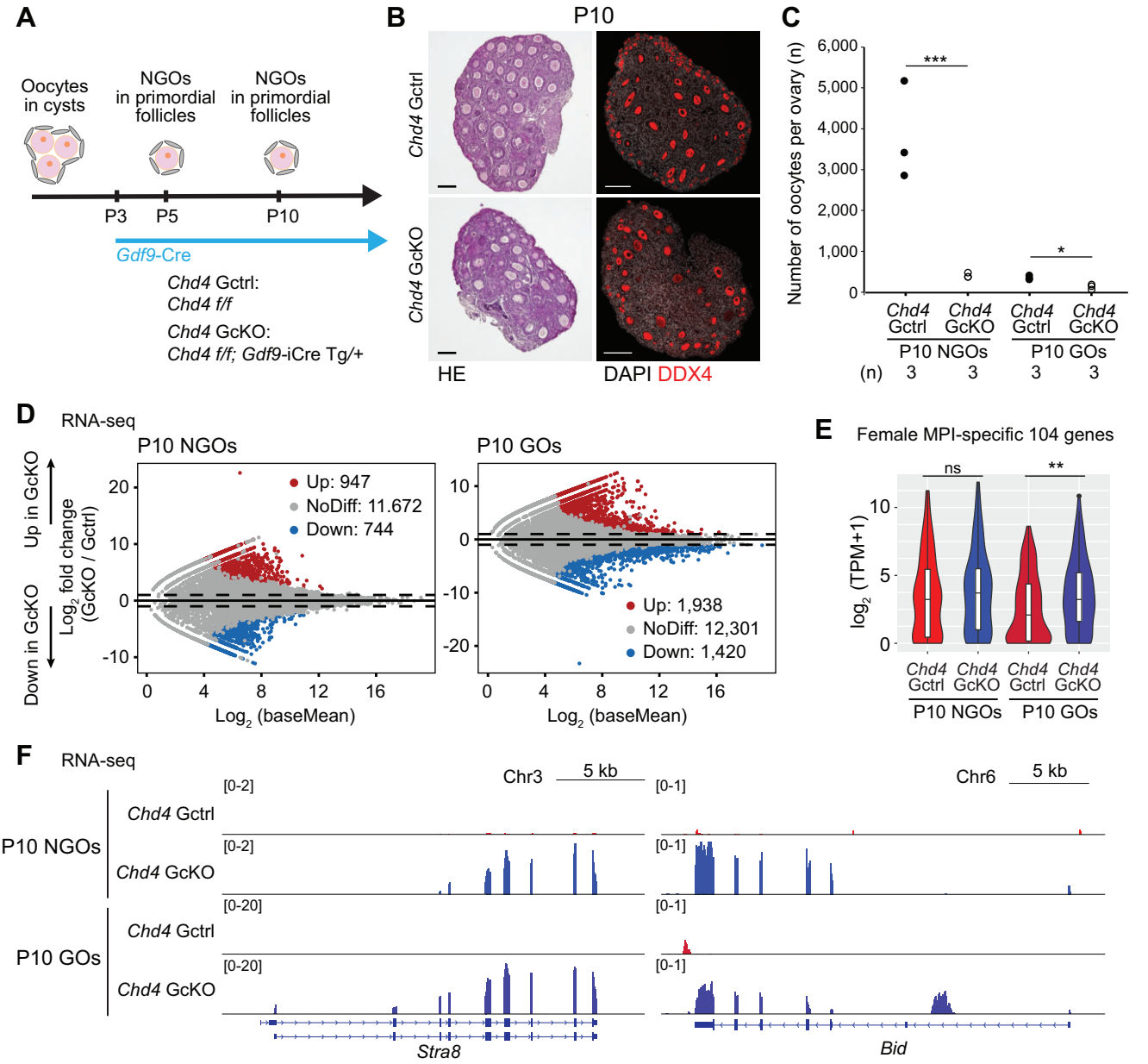

Figure 7. CHD4 is required for ovarian reserve maintenance. (**A**) Schematic for mouse models and experiments. (**B**) Ovarian sections of *Chd4* Gctrl and *Chd4* GcKO mice at P10. The sections were stained with hematoxylin and eosin or immunostained for DDX4 (red). Bars: 100 μm. Three mice were analyzed for each genotype at each time point, and representative images are shown. (**C**) Dot plots showing the estimated numbers of oocytes per ovary from *Chd4* Gctrl and *Chd4* GcKO mice at P10. At least three mice were analyzed for each genotype at each time point. Central bars represent mean values. $***P < 0.001$; $*P < 0.05$; two-tailed unpaired *t*-tests. (**D**) Comparison of RNA-seq data between *Chd4* Gctrl and *Chd4* GcKO NGOs and GOs at P10. A total of 500 NGOs and 100 GOs were isolated from P10 ovaries and were pooled as one replicate, and two independent biological replicates were examined for RNA-seq. DEGs (Log_2FoldChange > 1, *Padj* < 0.05, binominal test with Benjamini–Hochberg correction) are defined upregulated or downregulated in *Chd4* GcKO oocytes. (**E**) Violin plots with a Box plot indicate TPM values for female MPI-specific genes (104 genes) in *Chd4* Gctrl and *Chd4* GcKO oocytes at P10. The central lines represent medians. The upper and lower hinges correspond to the 25th and 75th percentiles. The upper and lower whiskers are extended from the hinge to the largest value no further than the 1.5× IQR from the hinge. $**P < 0.01$; ns, not significant; Wilcoxon rank sum test. (**F**) Track views showing RNA-seq signals in *Chd4* Gctrl and *Chd4* GcKO oocytes at P10, on the *Stra8* and *Bid* loci. The y-axis represents normalized tag counts for bulk RNA-seq in each sample. Data ranges are shown in brackets.

CHD4 is required for the maintenance of the ovarian reserve and oocyte survival

Because a critical aspect of ovarian reserve is the long maintenance of chromatin states during the female reproductive life span, we next determined whether CHD4 is required for maintenance of ovarian reserve after its establishment. To elucidate the function of CHD4 in the maintenance of NGOs in the ovarian reserve, we generated another line of CHD4 conditional knockout mice using *Gdf9*-iCre, which is expressed NGOs from P3 (69) (*Chd4*$^{f/f}$; *Gdf9*-iCre $^{Tg/+}$; termed *Chd4* GcKO) (Figure 7A). CHD4 was localized in the nuclei of NGOs in primordial follicles and GOs in primary follicles of P10 ovaries, and nearly complete depletion of CHD4 was observed in P10 *Chd4* GcKO oocytes

(Supplementary Figure S3A and B). In P10 ovaries in which primordial follicle formation is complete, the estimated numbers of NGOs and GOs in the ovaries of *Chd4* GcKO mice were significantly reduced compared to *Chd4* Gctrl mice (Figure 7B and C). These results indicate that CHD4 is essential for the maintenance of NGOs and the survival of GOs.

To determine the function of CHD4 in maintenance of ovarian reserve and survival of GOs, NGOs and GOs were isolated from P10 ovaries, and RNA-seq analysis was performed (Supplementary Figure S3C). In the P10 *Chd4* GcKO NGOs, 947 genes were upregulated, and 744 genes were downregulated [Figure 7D (left) and Supplementary Dataset S4]. In the P10 *Chd4* GcKO GOs, 1938 genes were upregulated, and 1420 genes were downregulated [Figure 7D (right) and Supplementary Dataset S4]. GO enrichment analyses show that upregulated genes in P10 *Chd4* GcKO NGOs were associated with apoptotic cell clearance (Supplementary Figure S3D). In addition, upregulated genes in P10 *Chd4* GcKO GOs were enriched with genes involved in synaptonemal complex assembly, which is related to MPI (Supplementary Figure S3D). Female MPI-specific genes were upregulated in *Chd4* GcKO GOs (Figure 7E). Similar to *Chd4* DcKO, *Stra8* expression was increased in both P10 NGOs and GOs in *Chd4* GcKO [Figure 7F (left)]. We also examined apoptosis-related genes and found that the expression of a pro-apoptotic gene, *Bid* (70), a key player in apoptosis, was increased in both NGOs and GOs in *Chd4* GcKO [Figure 7F (right)]. In summary, CHD4 is essential for oocyte survival and maintenance of ovarian reserve by repressing a group of the MPI genes and apoptosis genes.

CHD4 repressed apoptosis-related genes for male germ cell survival

After determining the function of CHD4 in the female germline, we finally sought to address whether CHD4 has a common function in the female and male germline. In the male germline, around the time of birth, mitotically arrested prospermatogonia resume active cell cycle and transition to spermatogonia after birth, which sustains long-term fertility of males by stem self-renewal (71). Recent studies using germline-specific conditional knockout of *Chd4* revealed that CHD4 is required for the survival of undifferentiated spermatogonia (24,25). Consistent with these studies, our *Chd4* DcKO males (Figure 8A) showed germ cell depletion that became evident at P3 testes (Figure 8B).

To examine the genes regulated by CHD4, we isolated undifferentiated male germ cells from P3 testes using a previously established FACS method (72,73) and performed RNA-seq analysis (Supplementary Figure S4A). In P3 *Chd4* DcKO male germ cells, 696 genes were upregulated and 168 genes were downregulated (Figure 8C and Supplementary Dataset S5). GO enrichment analyses revealed that the genes upregulated in *Chd4* DcKO male germ cells were associated with 'cell morphogenesis' and 'regulation of secretion by cell' (Supplementary Figure S4B). Next, we examined whether the expression of MPI genes is upregulated by *Chd4* deletion, as observed in oocytes, but found no difference in the expression of 104 female MPI genes (Supplementary Figure S4C). However, pro-apoptotic genes *Bbc3* and *Gadd45g* were upregulated in *Chd4* DcKO male germ cells, as was observed in oocytes (Figure 8D and Supplementary Figure S4D). Thus, CHD4 represses the *Bbc3* and *Gadd45* genes in both males and females.

To determine whether CHD4 also represses accessible chromatin in male germ cells, we performed ATAC-seq analysis on P3 *Chd4* DcKO male germ cells (Supplementary Figure S4E). Chromatin accessibility was increased in *Chd4* DcKO male germ cells compared to P3 *Chd4* Dctrl, as observed in oocytes (Figure 8E). In addition, P3 *Chd4* DcKO male germ cell-specific ATAC peaks were enriched in intron and intergenic regions, and only slightly in the promoter-TSS region (Figure 8F). As shown in the track view, chromatin accessibility of the *Bbc3* gene at the TSS was increased (Figure 8D). These results indicate that CHD4 suppresses expression of apoptosis genes by repressing chromatin accessibility in P3 *Chd4* DcKO male germ cells, leading to cell survival. Taken together, we conclude that CHD4 defines the chromatin state to ensure germ cell survival, enabling the long-term maintenance of female and male germ cells.

Discussion

The germline must maintain genome integrity to ensure generation of the offspring. Thus, mechanisms underlying long-term maintenance of the germline are critical at sexually dimorphic stages of the germline: one for maintenance of the ovarian reserve in females and another for maintenance of spermatogonial stem cells in males. We report here that CHD4 is a critical regulator for the long-term maintenance of the germline in both males and females. In combination with mouse genetics and epigenomic analyses, our study reveals that CHD4 directly binds and closes accessible chromatin at the distal regulatory elements genome-wide. This mechanism underlies regulation of pro-apoptotic genes in both females and males (Figure 8G). Notably, the female germline is maintained in the ovarian reserve after MPI, and CHD4 is required to close the regulatory elements for MPI genes in females but not in males (Figure 8G). These results highlight the common and distinct features of chromatin regulation in female and male germlines.

We find that CHD4 is required for both formation and maintenance of ovarian reserve. Because CHD4 has a maintenance function after ovarian reserve formation, it is likely that CHD4 continues to associate with chromatin in MPI-arrested NGOs. The histone H3.3 chaperone HIRA, which continues to replace H3.3 in NGOs is critical to maintain the ovarian reserve (74), suggesting that the chromatin state of NGOs is not static. Thus, a chromatin remodeler may be required to maintain a dynamic chromatin environment in NGOs. Furthermore, loss of the DNA damage response (DDR) genes has been implicated in ovarian aging, suggesting a possible function of DDR in the ovarian reserve maintenance (75). Noteworthy is that CHD4 is known to function in the context of DDR (76,77). To further clarify the molecular mechanism for CHD4 in formation and maintenance of the ovarian reserve, the composition of the CHD4-containing chromatin remodeling complex needs to be determined to distinguish its function from other chromatin remodelers whose functions are not known in ovarian reserve formation.

Another critical regulator of POT is PRC1 for MPI exit (7). Notably, MPI genes repressed by CHD4 (Figure 3D) are also repressed by PRC1 (7), suggesting possible coordination between CHD4 and PRC1 in MPI exit. In this context, CHD4 closes the accessible chromatin at POT. Consistent with this observation, in embryonic stem cells, CHD4-containing NuRD complexes deacetylate histone H3K27 and

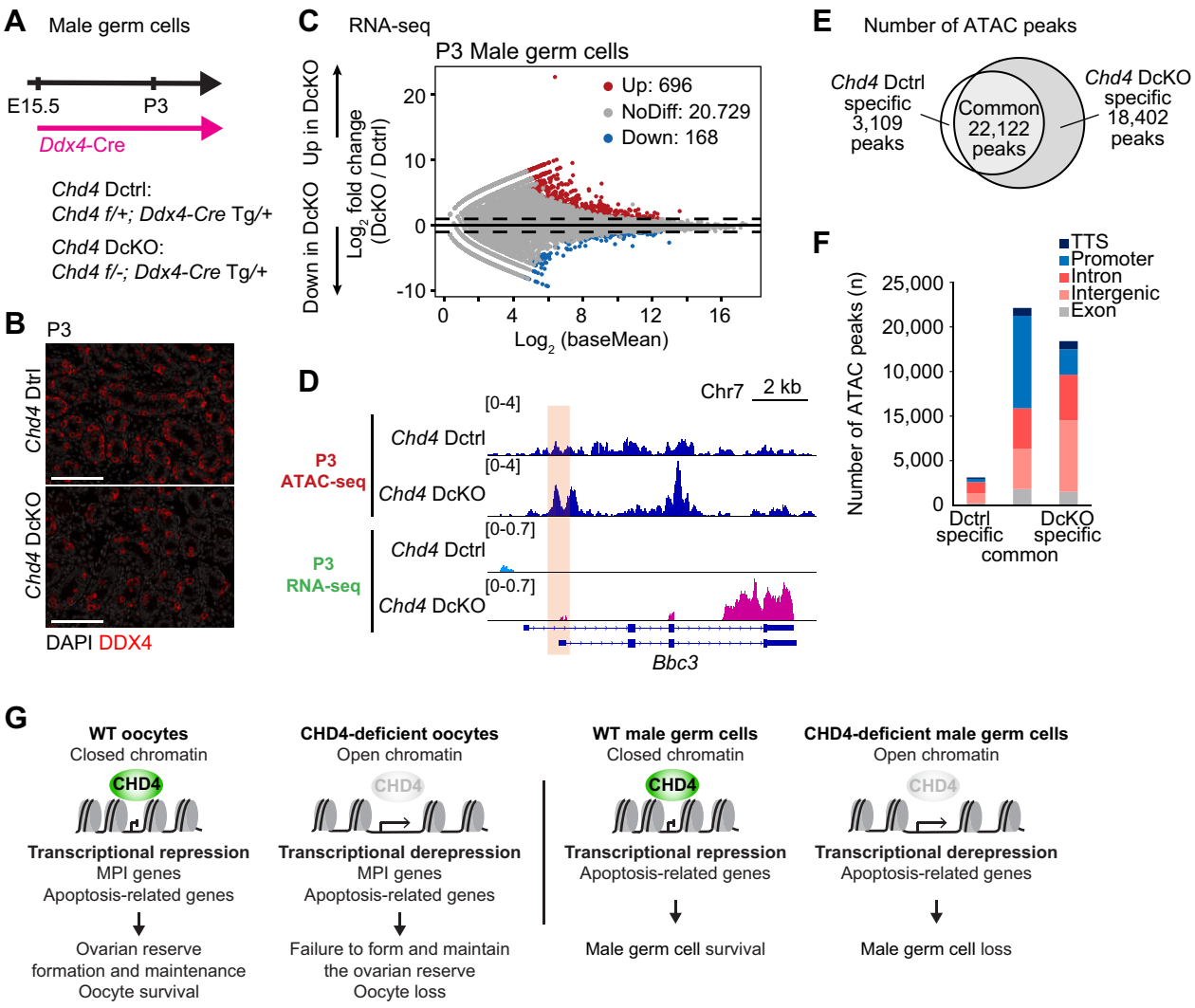

Figure 8. CHD4 suppresses pro-apoptotic genes for male germ cell survival, and summary model. (**A**) Schematic for mouse models and experiments. (**B**) Immunostaining of DDX4 in testicular sections in *Chd4* Dctrl and *Chd4* DcKO at P3. Bars: 100 μm. Three mice were analyzed for each genotype at each time point, and representative images are shown. (**C**) Comparison of RNA-seq data between *Chd4* Dctrl and *Chd4* DcKO undifferentiated male germ cells at P3. Two independent biological replicates were examined for RNA-seq. DEGs (Log_2FoldChange > 1, *Padj* < 0.05, binominal test with Benjamini–Hochberg correction) are are defined upregulated or downregulated in *Chd4* DcKO undifferentiated male germ cells. (**D**) Representative track views of *Bbc3* locus in P3 undifferentiated male germ cells of indicated genotypes. Data ranges are shown in brackets. Specific ATAC-seq peak regions in *Chd4* DcKO are highlighted. (**E**) Venn diagram indicates overlap of ATAC-seq peaks between *Chd4* Dctrl and *Chd4* DcKO undifferentiated male germ cells at P3. (**F**) Numbers and genomic distribution of ATAC-seq peaks shown in panel (E). (**G**) Model of CHD4's function in oocytes and undifferentiated male germ cells.

recruit PRC2, which often functions with PRC1 to facilitate H3K27me3-mediated repression (78). On the other hand, CHD4 was also enriched at downregulated genes in *Chd4* DcKO NGOs at P1 and P5 (Figure 6E), suggesting the possible function of CHD4 in gene activation. Indeed, CHD4 not only represses transcription, but the CHD4-containing NuRD complex also functions in gene activation in stem cells and during development and is required for expression of genes required for stem cell maintenance (17,27,79). We found that genes involved in oogenesis, such as *Gdf9* and *Zp3*, were downregulated in *Chd4* DcKO NGOs. These results suggest that CHD4 regulates the expression of key genes that define the identity of each cell type.

We also investigated the target sites of CHD4-mediated chromatin remodeling. The majority of CHD4 binding sites and the accessible chromatin sites closed by CHD4 are located in intergenic regions and introns. To determine the most enriched DNA motifs at sites closed by CHD4 in wild-type (i.e. CHD4-mediated transcriptional repression), we performed a *de novo* motif analysis of cKO-specific ATAC peaks in both females and males (Supplementary Figure S4F). In females, the PRDM9 motif, which is often a feature of meiotic recombination sites, was highly enriched, consistent with the role of CHD4 in facilitating exit from the MPI program. The ZNF11 motif was commonly enriched in both females and males, suggesting a common program between males and females. Intriguingly, the NFYB and POU3F1 motifs, detected in males, become open in late spermatogenesis (80). Thus, it is tempting to speculate that the regulatory elements used in late spermatogenesis are remodeled by CHD4 at an early stage, which may represent a mechanism for epigenetic priming in the male germline (81).

To further characterize CHD4 binding sites, we performed a motif analysis in the regions of CHD4 CUT&Tag peaks for P5 oocytes (Supplementary Figure S5A). We detected motifs for transcription factors whose function is not known in the germline. However, *de novo* motifs detected common motifs for basic helix-loop-helix family, basic leucine zipper family and homeobox family. We further performed HOMER *de novo* motif analysis of CHD4 CUT&Tag peaks in TSSs (±1 kb) of DEG in *Chd4* Dctrl and *Chd4* DcKO oocytes at P1 and P5 (Supplementary Figure S5B). The analysis detected *de novo* motifs have *P*-values with the possibility of false positives, suggesting that there are no specific DNA sequences enriched for activation and inhibition of transcription. These results suggest that CHD4 recognizes a wide variety of DNA sequences depending on the protein complexes in which CDH4 exists.

CHD4 is required to maintain stem cell identity by restricting the expression of differentiation-associated genes (17,82,83). The CHD4-containing ChAHP complex is a critical determinant of 3D chromatin (84), and CHD4 regulates cell differentiation by preventing enhancer activation through enhancer-promoter interactions (85,86). This mechanism may underlie the function of CHD4 in the germline, which has a marked similarity to the function of CHD4 in maintaining herpesvirus latency (87–89). In human cells, CHD4 is required for the maintenance of Kaposi's sarcoma-associated herpesvirus (KSHV)-mediated latent infection, in which viral genes are poised to be transcribed in the latent chromatin (87). During latent infection, CHD4 binds and inhibits the enhancers that are derived from KSHV's terminal repeats and prevents expression of viral genes (89), and the cleavage of the CHD4 protein is linked to cell apoptosis (88). Thus, CHD4 functions to maintain the cellular state, and this function may be critical for maintaining the ovarian reserve and epigenetic priming in the germline. Given the similarity to latent infection, it would be interesting to determine whether CHD4 cleavage triggers apoptosis in oogenesis.

Together, our study reveals a chromatin remodeling mechanism underlying regulatory elements required for key developmental transitions in the germline. A next key question is how these specific sites are determined to be regulated by CHD4. Because transcription factors (FIGLA, FOXO3) and several signaling pathways (Notch, TGF-β, JNK and hypoxia signaling) are implicated in primordial follicle formation, it will be important to understand how these mechanisms intersect with chromatin remodeling to establish the necessary chromatin states for ovarian reserve formation. Furthermore, given the significant role of the RNA regulatory network in primordial follicle formation (90), the mechanistic relationship between the RNA regulatory network and chromatin-based cellular memory emerges as an important agenda for future investigation.

Data availability

The raw data of quantifications presented in the main figures and supplementary figures are provided as 'Source data files'. RNA-seq data reported in this study were deposited to the Gene Expression Omnibus (accession no. GSE273309). Source data are provided with this paper.

Supplementary data

Supplementary Data are available at NAR Online.

Acknowledgements

We thank T. Broering and H. Abe for their contribution to the initial stage of this project and members of the Namekawa laboratory for discussion and helpful comments regarding this manuscript. We also thank N. Hunter, T. Yoshida and Y. Izumiya for discussion, K. Georgopoulos for providing the *Chd4* floxed mice, M. A. Surani for providing *Stella*-GFP transgenic mice, S. Maezawa for providing the homemade Tn5 transposase for ATAC-seq and A. Toth for providing the HORMAD1 antibody.

Author contributions: Y.M. and S.H.N. designed the study. Y.M., M.H., Y.K., R.G.D., A.L.B. and A.S.F. performed experiments and analyzed the data. Y.M., M.H., Y.K., R.G.D., R.M.S. and S.H.N. interpreted the results. Y. M., R.M.S. and S.H.N wrote the manuscript with critical feedback from M.H. and Y.K. R.M.S. and S.H.N. supervised the project.

Funding

Japan Society for Promotion of Science [Overseas Research Fellowships to Y.M.]; Lalor Foundation; Global Consortium for Reproductive Longevity and Equality [2223 to Y.M.]; UC Davis; NIH [R35 GM141085 to S.H.N and R21 HD110146 to S.H.N and R.M.S]. Funding for open access charge: UC Davis Startup Fund.

Conflict of interest statement

None declared.

References

1. Grive,K.J. and Freiman,R.N. (2015) The developmental origins of the mammalian ovarian reserve. *Development*, **142**, 2554–2563.
2. Ford,E.A., Beckett,E.L., Roman,S.D., McLaughlin,E.A. and Sutherland,J.M. (2020) Advances in human primordial follicle activation and premature ovarian insufficiency. *Reproduction*, **159**, R15–R29.
3. Hancock,G.V., Wamaitha,S.E., Peretz,L. and Clark,A.T. (2021) Mammalian primordial germ cell specification. *Development*, **148**, dev189217.
4. Martínez-Marchal,A., Huang,Y., Guillot-Ferriols,M.T., Ferrer-Roda,M., Guixé,A., Garcia-Caldés,M. and Roig,I. (2020) The DNA damage response is required for oocyte cyst breakdown and follicle formation in mice. *PLoS Genet.*, **16**, e1009067.
5. Tharp,M.E., Malki,S. and Bortvin,A. (2020) Maximizing the ovarian reserve in mice by evading LINE-1 genotoxicity. *Nat. Commun.*, **11**, 330.
6. Niu,W. and Spradling,A.C. (2022) Mouse oocytes develop in cysts with the help of nurse cells. *Cell*, **185**, 2576–2590.
7. Hu,M., Yeh,Y.H., Munakata,Y., Abe,H., Sakashita,A., Maezawa,S., Vidal,M., Koseki,H., Hunter,N., Schultz,R.M., *et al.* (2022) PRC1-mediated epigenetic programming is required to generate the ovarian reserve. *Nat. Commun.*, **13**, 4510.
8. Hu,M., Schultz,R.M. and Namekawa,S.H. (2023) Epigenetic programming in the ovarian reserve. *Bioessays*, **45**, e2300069.
9. Soyal,S.M., Amleh,A. and Dean,J. (2000) FIGalpha, a germ cell-specific transcription factor required for ovarian follicle formation. *Development*, **127**, 4645–4654.
10. Trombly,D.J., Woodruff,T.K. and Mayo,K.E. (2009) Suppression of Notch signaling in the neonatal mouse ovary decreases primordial follicle formation. *Endocrinology*, **150**, 1014–1024.
11. Patton,B.K., Madadi,S. and Pangas,S.A. (2021) Control of ovarian follicle development by TGFβ family signaling. *Curr. Opin. Endocr. Metab. Res.*, **18**, 102–110.

12. Niu,W., Wang,Y., Wang,Z., Xin,Q., Wang,Y., Feng,L., Zhao,L., Wen,J., Zhang,H., Wang,C., *et al.* (2016) JNK signaling regulates E-cadherin junctions in germline cysts and determines primordial follicle formation in mice. *Development*, **143**, 1778–1787.
13. Shimamoto,S., Nishimura,Y., Nagamatsu,G., Hamada,N., Kita,H., Hikabe,O., Hamazaki,N. and Hayashi,K. (2019) Hypoxia induces the dormant state in oocytes through expression of Foxo3. *Proc. Natl Acad Sci. U.S.A.*, **116**, 12321–12326.
14. Clapier,C.R., Iwasa,J., Cairns,B.R. and Peterson,C.L. (2017) Mechanisms of action and regulation of ATP-dependent chromatin-remodelling complexes. *Nat. Rev. Mol. Cell Biol.*, **18**, 407–422.
15. Hota,S.K. and Bruneau,B.G. (2016) ATP-dependent chromatin remodeling during mammalian development. *Development*, **143**, 2882–2897.
16. Arends,T., Dege,C., Bortnick,A., Danhorn,T., Knapp,J.R., Jia,H., Harmacek,L., Fleenor,C.J., Straign,D., Walton,K., *et al.* (2019) CHD4 is essential for transcriptional repression and lineage progression in B lymphopoiesis. *Proc. Natl Acad Sci. U.S.A.*, **116**, 10927–10936.
17. Zhao,H., Han,Z., Liu,X., Gu,J., Tang,F., Wei,G. and Jin,Y. (2017) The chromatin remodeler Chd4 maintains embryonic stem cell identity by controlling pluripotency- and differentiation-associated genes. *J Biol. Chem.*, **292**, 8507–8519.
18. O'Shaughnessy-Kirwan,A., Signolet,J., Costello,I., Gharbi,S. and Hendrich,B. (2015) Constraint of gene expression by the chromatin remodelling protein CHD4 facilitates lineage specification. *Development*, **142**, 2586–2597.
19. Yoshida,T., Hu,Y., Zhang,Z., Emmanuel,A.O., Galani,K., Muhire,B., Snippert,H.J., Williams,C.J., Tolstorukov,M.Y., Gounari,F., *et al.* (2019) Chromatin restriction by the nucleosome remodeler Mi-2β and functional interplay with lineage-specific transcription regulators control B-cell differentiation. *Genes Dev.*, **33**, 763–781.
20. Hoffmeister,H., Fuchs,A., Erdel,F., Pinz,S., Gröbner-Ferreira,R., Bruckmann,A., Deutzmann,R., Schwartz,U., Maldonado,R., Huber,C., *et al.* (2017) CHD3 and CHD4 form distinct NuRD complexes with different yet overlapping functionality. *Nucleic Acids Res.*, **45**, 10534–10554.
21. Ostapcuk,V., Mohn,F., Carl,S.H., Basters,A., Hess,D., Iesmantavicius,V., Lampersberger,L., Flemr,M., Pandey,A., Thomä,N.H., *et al.* (2018) Activity-dependent neuroprotective protein recruits HP1 and CHD4 to control lineage-specifying genes. *Nature*, **557**, 739–743.
22. Bornelöv,S., Reynolds,N., Xenophontos,M., Gharbi,S., Johnstone,E., Floyd,R., Ralser,M., Signolet,J., Loos,R., Dietmann,S., *et al.* (2018) The nucleosome remodeling and deacetylation complex modulates chromatin structure at sites of active transcription to fine-tune gene expression. *Mol. Cell*, **71**, 56–72.
23. Ahel,J., Pandey,A., Schwaiger,M., Mohn,F., Basters,A., Kempf,G., Andriollo,A., Kaaij,L., Hess,D. and Bühler,M. (2024) ChAHP2 and ChAHP control diverse retrotransposons by complementary activities. *Genes Dev.*, **38**, 554–568.
24. Li,P., Tang,J., Yu,Z., Jin,C., Wang,Z., Li,M., Zou,D., Mang,X., Liu,J., Lu,Y., *et al.* (2022) CHD4 acts as a critical regulator in the survival of spermatogonial stem cells in mice. *Biol. Reprod.*, **107**, 1331–1344.
25. de Castro,R.O., Carbajal,A., Previato de Almeida,L., Goitea,V., Griffin,C.T. and Pezza,R.J. (2022) Mouse Chd4-NURD is required for neonatal spermatogonia survival and normal gonad development. *Epigenetics Chromatin*, **15**, 16.
26. Cafe,S.L., Skerrett-Byrne,D.A., De Oliveira,C.S., Nixon,B., Oatley,M.J., Oatley,J.M. and Lord,T. (2021) A regulatory role for CHD4 in maintenance of the spermatogonial stem cell pool. *Stem Cell Reports*, **16**, 1555–1567.
27. Williams,C.J., Naito,T., Arco,P.G., Seavitt,J.R., Cashman,S.M., De Souza,B., Qi,X., Keables,P., Von Andrian,U.H. and Georgopoulos,K. (2004) The chromatin remodeler Mi-2beta is required for CD4 expression and T cell development. *Immunity*, **20**, 719–733.
28. Gallardo,T., Shirley,L., John,G.B. and Castrillon,D.H. (2007) Generation of a germ cell-specific mouse transgenic Cre line, Vasa-Cre. *Genesis*, **45**, 413–417.
29. Payer,B., Lopes,Chuva de Sousa, Barton,S.M., Lee,S.C., Saitou,C. and Surani,M.A. (2006) Generation of stella-GFP transgenic mice: a novel tool to study germ cell development. *Genesis*, **44**, 75–83.
30. Pedersen,T. and Peters,H. (1968) Proposal for a classification of oocytes and follicles in the mouse ovary. *J. Reprod. Fertil.*, **17**, 555–557.
31. Yeh,Y.H., Hu,M., Nakagawa,T., Sakashita,A., Yoshida,S., Maezawa,S. and Namekawa,S.H. (2021) Isolation of murine spermatogenic cells using a violet-excited cell-permeable DNA binding dye. *J Vis. Exp.*, **167**, e61666.
32. Corces,M.R., Trevino,A.E., Hamilton,E.G., Greenside,P.G., Sinnott-Armstrong,N.A., Vesuna,S., Satpathy,A.T., Rubin,A.J., Montine,K.S., Wu,B., *et al.* (2017) An improved ATAC-seq protocol reduces background and enables interrogation of frozen tissues. *Nat. Methods*, **14**, 959–962.
33. Kaya-Okur,H.S., Wu,S.J., Codomo,C.A., Pledger,E.S., Bryson,T.D., Henikoff,J.G., Ahmad,K. and Henikoff,S. (2019) CUT&Tag for efficient epigenomic profiling of small samples and single cells. *Nat. Commun.*, **10**, 1930.
34. Kaya-Okur,H.S., Janssens,D.H., Henikoff,J.G., Ahmad,K. and Henikoff,S. (2020) Efficient low-cost chromatin profiling with CUT&Tag. *Nat. Protoc.*, **15**, 3264–3283.
35. Bolger,A.M., Lohse,M. and Usadel,B. (2014) Trimmomatic: a flexible trimmer for Illumina sequence data. *Bioinformatics*, **30**, 2114–2120.
36. Dobin,A., Davis,C.A., Schlesinger,F., Drenkow,J., Zaleski,C., Jha,S., Batut,P., Chaisson,M. and Gingeras,T.R. (2013) STAR: ultrafast universal RNA-seq aligner. *Bioinformatics*, **29**, 15–21.
37. Li,H., Handsaker,B., Wysoker,A., Fennell,T., Ruan,J., Homer,N., Marth,G., Abecasis,G. and Durbin,R. (2009) The Sequence Alignment/Map format and SAMtools. *Bioinformatics*, **25**, 2078–2079.
38. Liao,Y., Smyth,G.K. and Shi,W. (2014) featureCounts: an efficient general purpose program for assigning sequence reads to genomic features. *Bioinformatics*, **30**, 923–930.
39. Michael,F. (2002) Corrgrams. *Am. Stat.*, **56**, 316–324.
40. Love,M.I., Huber,W. and Anders,S. (2014) Moderated estimation of fold change and dispersion for RNA-seq data with DESeq2. *Genome Biol*, **15**, 550.
41. Zhou,Y., Zhou,B., Pache,L., Chang,M., Khodabakhshi,A.H., Tanaseichuk,O., Benner,C. and Chanda,S.K. (2019) Metascape provides a biologist-oriented resource for the analysis of systems-level datasets. *Nat. Commun.*, **10**, 1523.
42. Langmead,B. and Salzberg,S.L. (2012) Fast gapped-read alignment with Bowtie 2. *Nat. Methods*, **9**, 357–359.
43. Ramírez,F., Ryan,D.P., Grüning,B., Bhardwaj,V., Kilpert,F., Richter,A.S., Heyne,S., Dündar,F. and Manke,T. (2016) deepTools2: a next generation web server for deep-sequencing data analysis. *Nucleic Acids Res.*, **44**, W160–W165.
44. Zhang,Y., Liu,T., Meyer,C.A., Eeckhoute,J., Johnson,D.S., Bernstein,B.E., Nusbaum,C., Myers,R.M., Brown,M., Li,W., *et al.* (2008) Model-based analysis of ChIP-Seq (MACS). *Genome Biol.*, **9**, R137.
45. Quinlan,A.R. and Hall,I.M. (2010) BEDTools: a flexible suite of utilities for comparing genomic features. *Bioinformatics*, **26**, 841–842.
46. Heinz,S., Benner,C., Spann,N., Bertolino,E., Lin,Y.C., Laslo,P., Cheng,J.X., Murre,C., Singh,H. and Glass,C.K. (2010) Simple combinations of lineage-determining transcription factors prime cis-regulatory elements required for macrophage and B cell identities. *Mol. Cell*, **38**, 576–589.
47. Robinson,J.T., Thorvaldsdóttir,H., Winckler,W., Guttman,M., Lander,E.S., Getz,G. and Mesirov,J.P. (2011), Integrative genomics viewer. *Nat. Biotechnol.*, **29**, 24–26.

48. McLean,C.Y., Bristor,D., Hiller,M., Clarke,S.L., Schaar,B.T., Lowe,C.B., Wenger,A.M. and Bejerano,G. (2010) GREAT improves functional interpretation of cis-regulatory regions. *Nat. Biotechnol.*, **28**, 495–501.
49. John,G.B., Gallardo,T.D., Shirley,L.J. and Castrillon,D.H. (2008) Foxo3 is a PI3K-dependent molecular switch controlling the initiation of oocyte growth. *Dev. Biol.*, **321**, 197–204.
50. Soh,Y.Q., Junker,J.P., Gill,M.E., Mueller,J.L., van Oudenaarden,A. and Page,D.C. (2015) A gene regulatory program for meiotic prophase in the fetal ovary. *PLoS Genet.*, **11**, e1005531.
51. Romanienko,P.J. and Camerini-Otero,R.D. (2000) The mouse Spo11 gene is required for meiotic chromosome synapsis. *Mol. Cell*, **6**, 975–987.
52. Baudat,F., Manova,K., Yuen,J.P., Jasin,M. and Keeney,S. (2000) Chromosome synapsis defects and sexually dimorphic meiotic progression in mice lacking Spo11. *Mol. Cell*, **6**, 989–998.
53. de Vries,F.A., de Boer,E., van den Bosch,M., Baarends,W.M., Ooms,M., Yuan,L., Liu,J.G., van Zeeland,A.A., Heyting,C. and Pastink,A. (2005) Mouse Sycp1 functions in synaptonemal complex assembly, meiotic recombination, and XY body formation. *Genes Dev.*, **19**, 1376–1389.
54. Shin,Y.H., Choi,Y., Erdin,S.U., Yatsenko,S.A., Kloc,M., Yang,F., Wang,P.J., Meistrich,M.L. and Rajkovic,A. (2010) Hormad1 mutation disrupts synaptonemal complex formation, recombination, and chromosome segregation in mammalian meiosis. *PLoS Genet.*, **6**, e1001190.
55. Daniel,K., Lange,J., Hached,K., Fu,J., Anastassiadis,K., Roig,I., Cooke,H.J., Stewart,A.F., Wassmann,K., Jasin,M., *et al.* (2011) Meiotic homologue alignment and its quality surveillance are controlled by mouse HORMAD1. *Nat. Cell Biol.*, **13**, 599–610.
56. Kogo,H., Tsutsumi,M., Ohye,T., Inagaki,H., Abe,T. and Kurahashi,H. (2012) HORMAD1-dependent checkpoint/surveillance mechanism eliminates asynaptic oocytes. *Genes Cells*, **17**, 439–454.
57. Luo,M., Yang,F., Leu,N.A., Landaiche,J., Handel,M.A., Benavente,R., La Salle,S. and Wang,P.J. (2013) MEIOB exhibits single-stranded DNA-binding and exonuclease activities and is essential for meiotic recombination. *Nat. Commun.*, **4**, 2788.
58. Shibuya,H., Hernández-Hernández,A., Morimoto,A., Negishi,L., Höög,C. and Watanabe,Y. (2015) MAJIN links telomeric DNA to the nuclear membrane by exchanging telomere cap. *Cell*, **163**, 1252–1266.
59. Kanehisa,M. and Goto,S. (2000) KEGG: kyoto encyclopedia of genes and genomes. *Nucleic Acids Res.*, **28**, 27–30.
60. Lamkanfi,M. and Kanneganti,T.D. (2010) Caspase-7: a protease involved in apoptosis and inflammation. *Int. J Biochem. Cell Biol.*, **42**, 21–24.
61. Gonfloni,S., Di Tella,L., Caldarola,S., Cannata,S.M., Klinger,F.G., Di Bartolomeo,C., Mattei,M., Candi,E., De Felici,M., Melino,G., *et al.* (2009) Inhibition of the c-Abl-TAp63 pathway protects mouse oocytes from chemotherapy-induced death. *Nat. Med.*, **15**, 1179–1185.
62. Kerr,J.B., Hutt,K.J., Michalak,E.M., Cook,M., Vandenberg,C.J., Liew,S.H., Bouillet,P., Mills,A., Scott,C.L., Findlay,J.K., *et al.* (2012) DNA damage-induced primordial follicle oocyte apoptosis and loss of fertility require TAp63-mediated induction of Puma and Noxa. *Mol. Cell*, **48**, 343–352.
63. Lena,A.M., Rossi,V., Osterburg,S., Smirnov,A., Osterburg,C., Tuppi,M., Cappello,A., Amelio,I., Dötsch,V., De Felici,M., *et al.* (2021) The p63 C-terminus is essential for murine oocyte integrity. *Nat. Commun.*, **12**, 383.
64. ElInati,E., Zielinska,A.P., McCarthy,A., Kubikova,N., Maciulyte,V., Mahadevaiah,S., Sangrithi,M.N., Ojarikre,O., Wells,D., Niakan,K.K., *et al.* (2020) The BCL-2 pathway preserves mammalian genome integrity by eliminating recombination-defective oocytes. *Nat. Commun.*, **11**, 2598.
65. Goodman,J.V., Yamada,T., Yang,Y., Kong,L., Wu,D.Y., Zhao,G., Gabel,H.W. and Bonni,A. (2020) The chromatin remodeling enzyme Chd4 regulates genome architecture in the mouse brain. *Nat. Commun.*, **11**, 3419.
66. Graca Marques,J., Pavlovic,B., Ngo,Q.A., Pedot,G., Roemmele,M., Volken,L., Kisele,S., Perbet,R., Wachtel,M. and Schäfer,B.W. (2024) The chromatin remodeler CHD4 sustains ewing sarcoma cell survival by controlling global chromatin architecture. *Cancer Res.*, **84**, 241–257.
67. Buenrostro,J.D., Giresi,P.G., Zaba,L.C., Chang,H.Y. and Greenleaf,W.J. (2013) Transposition of native chromatin for fast and sensitive epigenomic profiling of open chromatin, DNA-binding proteins and nucleosome position. *Nat. Methods*, **10**, 1213–1218.
68. Kojima,M.L., de Rooij,D.G. and Page,D.C. (2019) Amplification of a broad transcriptional program by a common factor triggers the meiotic cell cycle in mice. *Elife*, **8**, e43738.
69. Lan,Z.J., Xu,X. and Cooney,A.J. (2004) Differential oocyte-specific expression of Cre recombinase activity in GDF-9-iCre, Zp3cre, and Msx2Cre transgenic mice. *Biol. Reprod.*, **71**, 1469–1474.
70. Korsmeyer,S.J., Wei,M.C., Saito,M., Weiler,S., Oh,K.J. and Schlesinger,P.H. (2000) Pro-apoptotic cascade activates BID, which oligomerizes BAK or BAX into pores that result in the release of cytochrome c. *Cell Death Differ.*, **7**, 1166–1173.
71. Yoshida,S. (2019) Heterogeneous, dynamic, and stochastic nature of mammalian spermatogenic stem cells. *Curr Top Dev. Biol.*, **135**, 245–285.
72. Nakagawa,T., Jörg,D.J., Watanabe,H., Mizuno,S., Han,S., Ikeda,T., Omatsu,Y., Nishimura,K., Fujita,M., Takahashi,S., *et al.* (2021) A multistate stem cell dynamics maintains homeostasis in mouse spermatogenesis. *Cell Rep.*, **37**, 109875.
73. Hu,M., Yeh,Y.H., Maezawa,S., Nakagawa,T., Yoshida,S. and Namekawa,S.H. (2024) PRC1 directs PRC2-H3K27me3 deposition to shield adult spermatogonial stem cells from differentiation. *Nucleic Acids Res.*, **52**, 2306–2322.
74. Nashun,B., Hill,P.W., Smallwood,S.A., Dharmalingam,G., Amouroux,R., Clark,S.J., Sharma,V., Ndjetehe,E., Pelczar,P., Festenstein,R.J., *et al.* (2015) Continuous histone replacement by hira is essential for normal transcriptional regulation and *de novo* DNA methylation during mouse oogenesis. *Mol. Cell*, **60**, 611–625.
75. Ruth,K.S., Day,F.R., Hussain,J., Martínez-Marchal,A., Aiken,C.E., Azad,A., Thompson,D.J., Knoblochova,L., Abe,H., Tarry-Adkins,J.L., *et al.* (2021) Genetic insights into biological mechanisms governing human ovarian ageing. *Nature*, **596**, 393–397.
76. O'Shaughnessy,A. and Hendrich,B. (2013) CHD4 in the DNA-damage response and cell cycle progression: not so NuRDy now. *Biochem. Soc. Trans.*, **41**, 777–782.
77. Broering,T.J., Alavattam,K.G., Sadreyev,R.I., Ichijima,Y., Kato,Y., Hasegawa,K., Camerini-Otero,R.D., Lee,J.T., Andreassen,P.R. and Namekawa,S.H. (2014) BRCA1 establishes DNA damage signaling and pericentric heterochromatin of the X chromosome in male meiosis. *J. Cell Biol.*, **205**, 663–675.
78. Kim,T.W., Kang,B.H., Jang,H., Kwak,S., Shin,J., Kim,H., Lee,S.E., Lee,S.M., Lee,J.H., Kim,J.H., *et al.* (2015) Ctbp2 modulates NuRD-mediated deacetylation of H3K27 and facilitates PRC2-mediated H3K27me3 in active embryonic stem cell genes during exit from pluripotency. *Stem Cells*, **33**, 2442–2455.
79. Yoshida,T., Hazan,I., Zhang,J., Ng,S.Y., Naito,T., Snippert,H.J., Heller,E.J., Qi,X., Lawton,L.N., Williams,C.J., *et al.* (2008) The role of the chromatin remodeler Mi-2beta in hematopoietic stem cell self-renewal and multilineage differentiation. *Genes Dev.*, **22**, 1174–1189.
80. Maezawa,S., Yukawa,M., Alavattam,K.G., Barski,A. and Namekawa,S.H. (2018) Dynamic reorganization of open chromatin underlies diverse transcriptomes during spermatogenesis. *Nucleic Acids Res.*, **46**, 593–608.
81. Kitamura,Y. and Namekawa,S.H. (2024) Epigenetic priming in the male germline. *Curr. Opin. Genet. Dev.*, **86**, 102190.

82. Sreenivasan,K., Rodríguez-delaRosa,A., Kim,J., Mesquita,D., Segalés,J., Arco,P.G., Espejo,I., Ianni,A., Di Croce,L., Relaix,F., *et al.* (2021) CHD4 ensures stem cell lineage fidelity during skeletal muscle regeneration. *Stem Cell Rep.*, **16**, 2089–2098.
83. Hirota,A., Nakajima-Koyama,M., Ashida,Y. and Nishida,E. (2019) The nucleosome remodeling and deacetylase complex protein CHD4 regulates neural differentiation of mouse embryonic stem cells by downregulating p53. *J Biol. Chem.*, **294**, 195–209.
84. Kaaij,L.J.T., Mohn,F., van der Weide,R.H., de Wit,E. and Bühler,M. (2019) The ChAHP complex counteracts chromatin looping at CTCF sites that emerged from SINE expansions in mouse. *Cell*, **178**, 1437–1451.
85. Marques,J.G., Gryder,B.E., Pavlovic,B., Chung,Y., Ngo,Q.A., Frommelt,F., Gstaiger,M., Song,Y., Benischke,K., Laubscher,D., *et al.* (2020) NuRD subunit CHD4 regulates super-enhancer accessibility in rhabdomyosarcoma and represents a general tumor dependency. *Elife*, **9**, e54993.
86. Goodman,J.V., Yamada,T., Yang,Y., Kong,L., Wu,D.Y., Zhao,G., Gabel,H.W. and Bonni,A. (2020) The chromatin remodeling enzyme Chd4 regulates genome architecture in the mouse brain. *Nat. Commun.*, **11**, 3419.
87. Kumar,A., Lyu,Y., Yanagihashi,Y., Chantarasrivong,C., Majerciak,V., Salemi,M., Wang,K.H., Inagaki,T., Chuang,F., Davis,R.R., *et al.* (2022) KSHV episome tethering sites on host chromosomes and regulation of latency-lytic switch by CHD4. *Cell Rep.*, **39**, 110788.
88. Miura,H., Wang,K.H., Inagaki,T., Chuang,F., Shimoda,M., Izumiya,C., Watanabe,T., Davis,R.R., Tepper,C.G., Komaki,S., *et al.* (2024) A LANA peptide inhibits tumor growth by inducing CHD4 protein cleavage and triggers cell death. *Cell Chem. Biol.*, **31**, 1909–1925.
89. Izumiya,Y., Algalil,A., Espera,J.M., Miura,H., Izumiya,C., Inagaki,T. and Kumar,A. (2024) Kaposi's sarcoma-associated herpesvirus terminal repeat regulates inducible lytic gene promoters. *J. Virol.*, **98**, e0138623.
90. Kato,Y., Iwamori,T., Ninomiya,Y., Kohda,T., Miyashita,J., Sato,M. and Saga,Y. (2019) ELAVL2-directed RNA regulatory network drives the formation of quiescent primordial follicles. *EMBO Rep.*, **20**, e48251.

Received: August 23, 2024. **Revised:** December 13, 2024. **Editorial Decision:** December 31, 2024. **Accepted:** January 6, 2025